Journal of Computational Physics 435 (2021) 110263

Contents lists available at ScienceDirect

Journal of Computational Physics

www.elsevier.com/locate/jcp

A new four-phase adaptive implicit method for compositional reservoir simulation

Bruno Ramon Batista Fernandes [a], Francisco Marcondes [b,*], Kamy Sepehrnoori [c]

[a] Center for Subsurface Energy and the Environment, The University of Texas at Austin, Austin, USA
[b] Department of Metallurgical Engineering and Material Science, Federal University of Ceará. Fortaleza, Brazil
[c] Hildebrand Department of Petroleum and Geosystems Engineering, The University of Texas at Austin. Austin, USA

ARTICLE INFO

Article history:
Available online 4 March 2021

Keywords:
Compositional reservoir simulation
AIM
IMPEC
Fully implicit
Stability analysis

ABSTRACT

Estimating oil and gas production from assets is essential to carry oil recovery processes. From the many techniques and tools used for such a task, the compositional simulation model is important for miscible displacement and problems with complex phase behavior. In this model, the fluid flow in porous media is described by a set of conservation equations. The solution of these problems involves spatial and time discretization schemes and approaches for handling the coupling of fluid flow and phase behavior. As a consequence, several solution algorithms arise from combining different selection of primary variables and equations, phase behavior decoupling techniques, and spatial/time discretization, which define the computational performance of these algorithms. In this work, a new Adaptive Implicit Method (AIM) is proposed by combining a global intensive variables Fully Implicit (FI) formulation and an IMPEC (IMplicit Pressure, Explicit Compositions) approach. In this approach, gridblocks are dynamically selected as FI or IMPEC based on a stability analysis algorithm. The fully implicit part considers pressure, water saturation, and overall compositions as primary variables and the IMPEC approach considers pressure and total number of moles for each component as primary variables. A new stability analysis algorithm is proposed and used for up to four-phases, but it is general enough to be used for any number of phases. The eigenvalues of the amplification matrix are used for the stability analysis and are computed using the Power's iteration method. The new approach is implemented in the in-house simulator called UTCOMPRS. The AIM formulation is compared to the fully implicit and IMPEC versions. We observed considerable improvement in the computational performance of UTCOMPRS with the new AIM when compared to the pure FI and IMPEC formulations.

1. Introduction

Predicting the fluid flow in porous media is important in the oil industry for forecasting the oil and gas production, allowing field optimization and uncertainty assessment. Reservoir simulators are one of the tools used to achieve such a goal and efforts have been devoted to improve the computational performance of these tools for different problems along the last few decades, which has allowed the use of more accurate models and better assessment of field opportunities. One of the ways for improving the performance of reservoir simulators is through the use of more efficient solution algorithms

* Corresponding author.
E-mail address: marcondes@ufc.br (F. Marcondes).

https://doi.org/10.1016/j.jcp.2021.110263
0021-9991/

for the coupling the fluid flow and phase behavior. Fully implicit (FI) algorithms have earned distinct attention in the literature due to its stability, which allows the construction more robust and fast simulators for practical oil reservoir problems. Furthermore, efforts have been concentrated in combining FI and explicit approaches, once it was realized that FI approaches do not need to be used in the whole reservoir domain. An approach that can dynamically select and use different implicitness is known as an Adaptive Implicit Method (AIM), and can result in a further speed-up of the solution. Adaptive implicit approaches are particularly successful in the compositional reservoir simulation, where several components may be used to characterize the hydrocarbon phases.

Since Fussel and Fussel [1], many formulations for the compositional reservoir simulation using Equation of State (EOS) and rigorous flash calculation have been proposed. IMplicit Pressure and Explicit Compositions (IMPEC) approaches, also known as IMplicit Pressure and Explicit Saturations (IMPES) and IMplicit Pressure and Explicit Mass (IMPEM), were used specially in research and in-house simulators since it is easier to include new physics in such formulations, and many authors have proposed different approaches by using different primary variables, pressure equation, and decoupling techniques [1–5]. In the IMPEC approach, only pressure is solved implicitly, resulting in a smaller Jacobian, while all other important unknowns are solved explicitly (i.e. saturations, mole concentrations, mass concentrations). Due to such explicitness, this approach will have its time-step size limited by numerical stability. Similarly, many FI approaches [6–9] and AIM [10,11] were proposed in the literature. From the FI approaches presented in the literature, one should highlight the natural variables formulation from Coats [7] and the global variables approach from Collins et al. [11]. In the natural variables, pressure, saturations, and some of the phase compositions are selected as primary variables. Such approach does not naturally decouple the flow equations from the phase equilibrium relations (fugacity equality), requiring a Gaussian elimination. On the other hand, when using the global variables approach from Collins et al. [11], the conservation equations are naturally decoupled, but an extra primary variable needs to be solved since it is based on an extensive variable set unlike the natural variables approach that is based on an intensive variable set. Recently, such drawback in the global variables FI approach was improved by transforming the original extensive variable set in an intensive one, which resulted in a good improvement of the global formulation [8]. The authors named the new formulation as PZS that stands after its primary variables (pressure, global molar fraction, and water saturation). This approach is one of the foundations of the work proposed here.

Thomas and Thurnau [12] observed that the stability issues of the IMPEC approach are concentrated in some specific areas of the reservoir, such as saturation front and regions around the producing and injecting wells. Based on this observation, Thomas and Thurnau [12] presented the first adaptive implicit method for the black-oil model. The authors used a matrix reduction to obtain the final form of the system of equations to be solved. The mathematical basis was presented in Thomas and Thurnau [13]. Despite of being the first method named as AIM in the petroleum industry, this method is not like the AIM commonly used in the literature, where the FI and the IMPEC formulations are combined. The first legitimate adaptive implicit approach is attributed to Forsyth and Sammon [14], who effectively combined implicit and explicit approaches without forcing elements of the Jacobian matrix to be null. The criteria for selecting gridblocks as FI or IMPEC are normally based on threshold values or stability analysis. Implicitness based on stability analysis can reduce unnecessary implicitness degree, since it provides a better way to select gridblocks based on the physics of the problem to be solved. Many authors have proposed and used different stability criteria for black-oil and compositional reservoir simulation [11,15–23]. However, to the best of our knowledge, there is no such development of adaptive implicit approaches for more than three phases. De Loubens et al. [24] presented a stability analysis for the case where phase mobilities are function of the velocities, such as in polymer flooding. The criterion was developed for a 1D single phase, non-Newtonian or non-Darcy flow, and it was implemented into an adaptive implicit simulator. Different algorithms are also available in the literature such as the adaptive multilevel space-time-stepping scheme (ADM-LTS) proposed by Carciopolo et al. [25], which makes use of a local time step approach to obtain better resolution in time. On this regard, the AIM does not provide any improvement in the time discretization resolution and is dependent on the order of approximation of both IMPEC and FI approaches involved (first order). However, the authors applied this approach for a simplified problem without mass transfer between the phases.

In this work, a new adaptive implicit method is proposed, implemented, and tested. The new AIM combines the PZS FI approach from Fernandes et al. [8] and the IMPEC version of the AIM from Collins et al. [11]. The original AIM version from Collins et al. [11] is also implemented and tested. The switching criterion for explicit saturations proposed by Coats [16] and originally designed for three phases is extended to any number of phases. Herein, the criterion has been tested to up to four-phases (water/oil/gas/second liquid hydrocarbon). The spectral radius of the amplification matrix is obtained using the Power's method [26]. The new scheme is implemented and tested in the University of Texas Compositional Reservoir Simulator (UTCOMPRS), a modified version of the UTCOMP simulator, originally developed by Chang [27].

2. Governing equations

In this paper, the compositional multiphase fluid flow in porous media is considered. The whole domain is assumed to be isothermal with no flow boundaries. No mass transfer between the aqueous phase and any of the hydrocarbon phases is considered. Local thermodynamic equilibrium is considered. Finally, the phase velocities are evaluated with the modified Darcy's law. Taking into account the above assumptions, the mole balance, for each hydrocarbon component, is obtained as

$$\frac{1}{V_b}\frac{\partial N_k}{\partial t} = \sum_{j=2}^{n_p}\left[-\vec{\nabla}\cdot(x_{kj}\xi_j\vec{u}_j) + \vec{\nabla}\cdot(\phi S_j \xi_j \overline{\overline{\Lambda}}_{kj}\cdot\vec{\nabla}x_{kj})\right] - \frac{\dot{q}_k}{V_b}, \quad k = 1,\ldots,n_c \tag{1}$$

and for water as

$$\frac{1}{V_b}\frac{\partial N_w}{\partial t} = -\vec{\nabla}\cdot(\xi_w\vec{u}_w) - \frac{\dot{q}_w}{V_b}, \tag{2}$$

where N_k is the total moles of component k, ξ_j is the molar density of phase j, V_b is the bulk volume, x_{kj} is the molar fraction of component k in phase j, $\dot{q}_k$ is the source/sink term of component k due to the producing/injecting well, S_j is the saturation of phase j, ϕ is the porosity, and $\overline{\overline{\Lambda}}_{kj}$ is the dispersion tensor of component i in phase j, n_p is the number of phases, n_c is the number of hydrocarbon components, and $\vec{u}_j$ is the velocity vector of phase j computed with the modified Darcy's law as

$$\vec{u}_j = -\frac{k_{rj}}{\mu_j}\overline{\overline{K}}\cdot(\vec{\nabla}P_j - \rho_j g\vec{\nabla}D), \quad j = 1,\ldots,n_p, \tag{3}$$

where $\overline{\overline{K}}$ is the absolute permeability tensor, k_{rj} is the relative permeability of phase j, and μ_j is the viscosity of phase j, ρ_j is the mass density of phase j, g is the gravity acceleration, D is the depth, and P_j is the pressure of phase j computed as

$$P_j = P + P_{cjo}, \quad j = 1,\ldots,n_p, \tag{4}$$

where P is the oil pressure and P_{cjo} is the capillary pressure of phase j with respect to the reference phase (oil), which is calculated using the Leverett J-function.

In this text, the subscript w stands for the water component or phase, and will be used interchangeably along with the subscripts 1, for aqueous phase, and $n_c + 1$ for the water component. Similarly, subscripts 2 and o stands for oil phase, 3 and g for gas phase, and 4 and l stand for the second oleic phase.

The volume constraint is also necessary and is written as

$$\phi = \frac{1}{V_b}\sum_{j=1}^{n_p}\frac{n_j}{\xi_j}, \tag{5}$$

where n_j is the number of moles of phase j.

The porosity is computed as

$$\phi = \phi^0\big(1 + C_f(P - P_{ref})\big), \tag{6}$$

where P_{ref} is a reference pressure, ϕ^0 is the reference porosity, and C_f is the rock compressibility.

The dispersion tensor is computed as the sum of the molecular diffusion and the mechanical dispersion as described in Bear [28] and Lake [29]. Dispersivities can be constant or a function of the gradient of the phase viscosities according to the model originally developed by Young [30].

The cubic EOS from Peng-Robinson [31] is used to accurately compute the densities and phase equilibrium of the hydrocarbon phases. An additional option for correcting the density of liquids using the volume shift parameter is also available. The phase behavior is computed in two stages: phase stability and flash calculation. First, the phase stability is performed to determine the number of hydrocarbon phases present in each gridblock. Two phase stability test algorithms are implemented in the UTCOMPRS simulator: the stationary point location method [32] and the Gibbs free energy minimization algorithm [33,34]. Finally, the flash calculation is performed for properly computing the phase compositions and phase mole fractions. In UTCOMPRS, the Accelerated Successive Substitution (ACSS) method [35] and a modified version of the Gibbs free energy minimization method [33] are combined in order to improve the flash calculation performance.

3. Approximate equations

In this work, we combine the fully implicit formulation proposed by Fernandes et al. [8] with the IMPEC formulation from Collins et al. [11]. The finite volume method is used to obtain the approximate equations for Cartesian grids. The time integral of the right-hand side of these equations is approximated at a time-level $n + \theta$, where $0 \leq \theta \leq 1$. Such approach, allows the user to switch among fully implicit and explicit variables. Integrating Eqs. (1) and (2) in time and for the control-volume of Fig. 1 and writing the result in a residual form yields

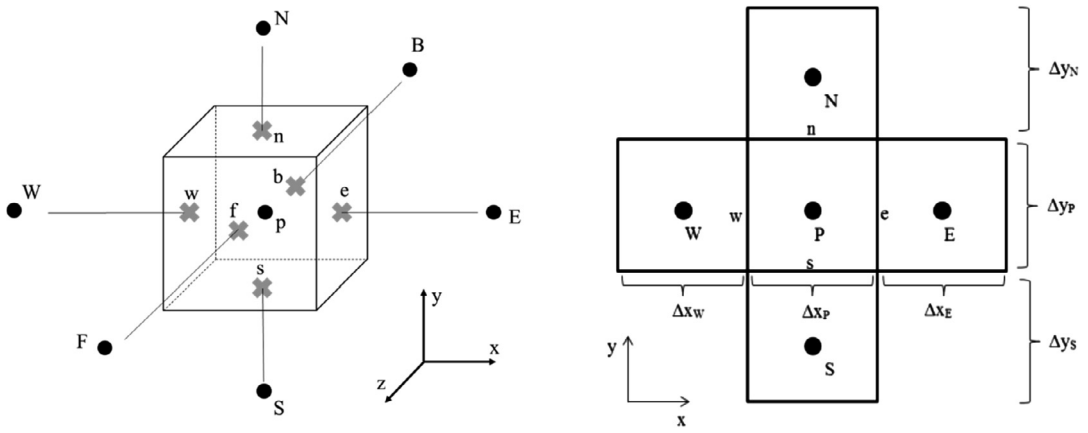

Fig. 1. Cartesian control-volume. (a) Three-dimensional view; (b) x–y plane.

$$R^N_{k,p} = -\left(N^{n+1}_{k,p} - N^n_{k,p}\right) + \Delta t \sum_{j=2}^{n_p}\left[F^{n+1}_{kj,e} - F^{n+1}_{kj,w} + F^{n+1}_{kj,n} - F^{n+1}_{kj,s} + F^{n+1}_{kj,f} - F^{n+1}_{kj,b}\right] + \Delta t \sum_{j=2}^{n_p}\left[J^{n+1}_{kj,e} - J^{n+1}_{kj,w} + J^{n+1}_{kj,n} - J^{n+1}_{kj,s} + J^{n+1}_{kj,f} - J^{n+1}_{kj,b}\right] - \Delta t \dot{q}^{n+1}_{k,p}, \quad k = 1, \ldots, n_c, \tag{7}$$

where $F_{kj,l}$ is the advective mole flux of component k in phase j through the interface l, $J_{kj,l}$ is the dispersive mole flux of component k in phase j through the interface l, and the superscript N denotes that this is a residue of the material balance equation. The advective mole fluxes, in each interface of an internal gridblock, are written as

$$F^{n+1}_{kj,e} = \left(x^{n+\theta}_{kj}\xi^{n+\theta}_j\lambda^{n+\theta}_j\right)_e T_e\left[P^{n+1}_E - P^{n+1}_p + P^{n+\theta}_{cjr,E} - P^{n+\theta}_{cjr,p} - \rho^{n+\theta}_{j,e} g(D_E - D_p)\right], \tag{8}$$

$$F^{n+1}_{kj,w} = \left(x^{n+\theta}_{kj}\xi^{n+\theta}_j\lambda^{n+\theta}_j\right)_w T_w\left[P^{n+1}_W - P^{n+1}_p + P^{n+\theta}_{cjr,W} - P^{n+\theta}_{cjr,p} - \rho^{n+\theta}_{j,w} g(D_W - D_p)\right], \tag{9}$$

$$F^{n+1}_{kj,n} = \left(x^{n+\theta}_{kj}\xi^{n+\theta}_j\lambda^{n+\theta}_j\right)_n T_n\left[P^{n+1}_N - P^{n+1}_p + P^{n+\theta}_{cjr,N} - P^{n+\theta}_{cjr,p} - \rho^{n+\theta}_{j,n} g(D_N - D_p)\right], \tag{10}$$

$$F^{n+1}_{kj,s} = \left(x^{n+\theta}_{kj}\xi^{n+\theta}_j\lambda^{n+\theta}_j\right)_s T_s\left[P^{n+1}_S - P^{n+1}_p + P^{n+\theta}_{cjr,S} - P^{n+\theta}_{cjr,p} - \rho^{n+\theta}_{j,s} g(D_S - D_p)\right], \tag{11}$$

$$F^{n+1}_{kj,f} = \left(x^{n+\theta}_{kj}\xi^{n+\theta}_j\lambda^{n+\theta}_j\right)_f T_f\left[P^{n+1}_F - P^{n+1}_p + P^{n+\theta}_{cjr,F} - P^{n+\theta}_{cjr,p} - \rho^{n+\theta}_{j,f} g(D_F - D_p)\right], \tag{12}$$

$$F^{n+1}_{kj,b} = \left(x^{n+\theta}_{kj}\xi^{n+\theta}_j\lambda^{n+\theta}_j\right)_b T_b\left[P^{n+1}_B - P^{n+1}_p + P^{n+\theta}_{cjr,B} - P^{n+\theta}_{cjr,p} - \rho^{n+\theta}_{j,b} g(D_B - D_p)\right], \tag{13}$$

where T_l is the transmissibility of the interface l, and θ can be chosen as either 0 or 1, depending on whether the gridblock is selected as FI or IMPEC, respectively.

The dispersive mole fluxes are computed as

$$J^{n+1}_{kj,e} = \Delta Y_p \Delta Z_p \left(\phi^{n+\theta}\xi^{n+\theta}_j S^{n+\theta}_j\right)_e \left[2\left(\Lambda^{n+\theta}_{xx,kj}\right)_e \frac{x^{n+\theta}_{kj,E} - x^{n+\theta}_{kj,p}}{\Delta X_p + \Delta X_E} + \left(\Lambda^{n+\theta}_{xy,kj}\right)_e \frac{x^{n+\theta}_{kj,Ne} - x^{n+\theta}_{kj,Se}}{\Delta Y_p + 0.5(\Delta Y_N + \Delta Y_S)} + \left(\Lambda^{n+\theta}_{xz,kj}\right)_e \frac{x^{n+\theta}_{kj,Fe} - x^{n+\theta}_{kj,Be}}{\Delta Z_p + 0.5(\Delta Z_F + \Delta Z_B)}\right], \tag{14}$$

$$J^{n+1}_{kj,w} = \Delta Y_p \Delta Z_p \left(\phi^{n+\theta}\xi^{n+\theta}_j S^{n+\theta}_j\right)_w \left[2\left(\Lambda^{n+\theta}_{xx,kj}\right)_w \frac{x^{n+\theta}_{kj,W} - x^{n+\theta}_{kj,p}}{\Delta X_p + \Delta X_W} + \left(\Lambda^{n+\theta}_{xy,kj}\right)_w \frac{x^{n+\theta}_{kj,Nw} - x^{n+\theta}_{kj,Sw}}{\Delta Y_p + 0.5(\Delta Y_N + \Delta Y_S)} + \left(\Lambda^{n+\theta}_{xz,kj}\right)_w \frac{x^{n+\theta}_{kj,Fw} - x^{n+\theta}_{kj,Bw}}{\Delta Z_p + 0.5(\Delta Z_F + \Delta Z_B)}\right], \tag{15}$$

$$J^{n+1}_{kj,n} = \Delta X_p \Delta Z_p \left(\phi^{n+\theta}\xi^{n+\theta}_j S^{n+\theta}_j\right)_n \left[2\left(\Lambda^{n+\theta}_{yy,kj}\right)_n \frac{x^{n+\theta}_{kj,N} - x^{n+\theta}_{kj,p}}{\Delta Y_p + \Delta Y_N} + \left(\Lambda^{n+\theta}_{xy,kj}\right)_n \frac{x^{n+\theta}_{kj,En} - x^{n+\theta}_{kj,Wn}}{\Delta X_p + 0.5(\Delta X_E + \Delta X_W)} + \left(\Lambda^{n+\theta}_{yz,kj}\right)_n \frac{x^{n+\theta}_{kj,Fn} - x^{n+\theta}_{kj,Bn}}{\Delta Z_p + 0.5(\Delta Z_F + \Delta Z_B)}\right], \tag{16}$$

$$J_{kj,s}^{n+1} = \Delta X_p \Delta Z_p \left(\phi^{n+\theta}\xi_j^{n+\theta} S_j^{n+\theta}\right)_s \left[2\left(\Lambda_{yy,kj}^{n+\theta}\right)_s \frac{x_{kj,S}^{n+\theta} - x_{kj,p}^{n+\theta}}{\Delta Y_p + \Delta Y_S} + \left(\Lambda_{xy,kj}^{n+\theta}\right)_s \frac{x_{kj,Es}^{n+\theta} - x_{kj,Ws}^{n+\theta}}{\Delta X_p + 0.5(\Delta X_E + \Delta X_W)} + \left(\Lambda_{yz,kj}^{n+\theta}\right)_s \frac{x_{kj,Fs}^{n+\theta} - x_{kj,Bs}^{n+\theta}}{\Delta Z_p + 0.5(\Delta Z_F + \Delta Z_B)} \right], \tag{17}$$

$$J_{kj,f}^{n+1} = \Delta X_p \Delta Y_p \left(\phi^{n+\theta}\xi_j^{n+\theta} S_j^{n+\theta}\right)_f \left[2\left(\Lambda_{zz,kj}^{n+\theta}\right)_f \frac{x_{kj,F}^{n+\theta} - x_{kj,p}^{n+\theta}}{\Delta Z_p + \Delta Z_F} + \left(\Lambda_{xz,kj}^{n+\theta}\right)_f \frac{x_{kj,Ef}^{n+\theta} - x_{kj,Wf}^{n+\theta}}{\Delta X_p + 0.5(\Delta X_E + \Delta X_W)} + \left(\Lambda_{yz,kj}^{n+\theta}\right)_f \frac{x_{kj,Nf}^{n+\theta} - x_{kj,Sf}^{n+\theta}}{\Delta Y_p + 0.5(\Delta Y_N + \Delta Y_S)} \right], \tag{18}$$

$$J_{kj,b}^{n+1} = \Delta X_p \Delta Y_p \left(\phi^{n+\theta}\xi_j^{n+\theta} S_j^{n+\theta}\right)_b \left[2\left(\Lambda_{zz,kj}^{n+\theta}\right)_b \frac{x_{kj,B}^{n+\theta} - x_{kj,p}^{n+\theta}}{\Delta Z_p + \Delta Z_B} + \left(\Lambda_{xz,kj}^{n+\theta}\right)_b \frac{x_{kj,Eb}^{n+\theta} - x_{kj,Wb}^{n+\theta}}{\Delta X_p + 0.5(\Delta X_E + \Delta X_W)} + \left(\Lambda_{yz,kj}^{n+\theta}\right)_b \frac{x_{kj,Nb}^{n+\theta} - x_{kj,Sb}^{n+\theta}}{\Delta Y_p + 0.5(\Delta Y_N + \Delta Y_S)} \right]. \tag{19}$$

Notice that the pressure in Eqs. (8) through (13) are always approximated at the next time-level (implicit). Thus, the formulation is reduced to IMPEC when $\theta = 0$. Also, it is important to notice that the value of theta θ changes for every gridblock. Therefore, if the value of θ is 0 for gridblock p and 1 for gridblock E, the fluxes across interface e will have properties from gridblock p evaluated explicitly and properties from gridblock E evaluated implicitly.

The dispersion tensor components are approximated using the approach presented in Chang [27]. Also, advective and dispersive fluxes across interfaces at the reservoir boundaries are null.

No matter if a gridblock is set as IMPEC or fully implicit, the volume constraint equation is always treated as using a fully implicit formulation. The volume constraint equation, written in a residual form is given as

$$R_p^P = \sum_{j=1}^{n_p} \frac{n_{j,p}^{n+1}}{\xi_{j,p}^{n+1}} - V_{b,p}\phi_p^{n+1}. \tag{20}$$

Details on the computation of mole rates for the wells can be found on Fernandes [36] and Chang [27].

4. The adaptive implicit formulation

The (PZS) formulation of Fernandes et al. [8] consists of the formulation proposed by Collins et al. [11] with a change in the primary variable set from $\{P, N_i\}$ to $\{P, Z_i, N_T, S_w\}$, where N_T is the total number of moles, Z_i refers to $n_c - 1$ overall compositions, and S_w is the water saturation. In this approach, a Gauss elimination is performed to eliminate N_T from the linear system, where N_T is obtained after solving for the PZS primary variable set $\{P, Z_i, S_w\}$. Therefore, the change of variables presented by Fernandes et al. [8] needs to be performed for the FI gridblocks. For the IMPEC gridblocks, it is also performed a gaussian elimination to reduce the unknowns just to the gridblock pressure. Also, the primary variables set for the FI and the IMPEC formulations are different. For the FI gridblocks, the primary variables are $\{P, Z_i, S_w\}$, while for the IMPEC gridblocks the primary variables are $\{P, N_i\}$.

The Newton Raphson method is used considering the pressure and total number moles as primary variables, following the approach from Collins et al. [11]:

$$\overline{\overline{J}}_k^{n+1} \Delta\vec{x}_k^{n+1} = -\vec{r}_k^{n+1}, \tag{21}$$

where $\Delta\vec{x}_k^{n+1}$ are the changes in the primary variables at iteration k, $\vec{r}_k^{n+1}$ are the residues of the volume balance and material balance equations at iteration k, and $\overline{\overline{J}}_k^{n+1}$ is the Jacobian matrix at iteration k. For a 1D problem, Eq. (21) is illustrated using a blocked Jacobian, blocked unknowns vector, and blocked residues vector as given below:

$$\begin{bmatrix} J_{1,P} & J_{1,E} & & & & \\ J_{2,W} & J_{2,P} & J_{2,E} & & & \\ & \ddots & \ddots & \ddots & & \\ & & J_{N_B-1,W} & J_{N_B-1,P} & J_{N_B-1,E} & \\ & & & J_{N_B,W} & J_{N_B,P} & \end{bmatrix} \begin{bmatrix} \Delta X_1 \\ \Delta X_2 \\ \vdots \\ \Delta X_{N_B-1} \\ \Delta X_{N_B} \end{bmatrix} = - \begin{bmatrix} R_1 \\ R_2 \\ \vdots \\ R_{N_B-1} \\ R_{N_B} \end{bmatrix}, \tag{22}$$

where, using Collins et al. [11], formulation we have

Fig. 2. 1D grid illustrations.

	P	N_1	N_2	N_3	N_w	P	N_1	N_2	N_3	N_w	P	N_1	N_2	N_3	N_w	P	N_1	N_2	N_3	N_w
R^P	X	X	X	X	X															
R_1^N	X	X	X	X	X	X														
R_2^N	X	X	X	X	X	X														
R_3^N	X	X	X	X	X	X														
R_w^N	X	X	X	X	X	X														
R^P						X	X	X	X	X										
R_1^N	X	X	X	X	X	X	X				X									
R_2^N	X	X	X	X	X	X		X			X									
R_3^N	X	X	X	X	X	X			X		X									
R_w^N	X	X	X	X	X	X				X	X									
R^P											X	X	X	X	X					
R_1^N						X					X	X				X	X	X	X	X
R_2^N						X					X		X			X	X	X	X	X
R_3^N						X					X			X		X	X	X	X	X
R_w^N						X					X				X	X	X	X	X	X
R^P																X	X	X	X	X
R_1^N											X					X	X	X	X	X
R_2^N											X					X	X	X	X	X
R_3^N											X					X	X	X	X	X
R_w^N											X					X	X	X	X	X

Fig. 3. Illustration of the Jacobian obtained using the Collins et al. [11] formulation for a 1D grid with four grid-blocks and three hydrocarbon components plus water.

$$J_{ij} = \begin{bmatrix} \frac{\partial R_i^P}{\partial P_j} & \frac{\partial R_i^P}{\partial N_{1j}} & \cdots & \frac{\partial R_i^P}{\partial N_{n_c j}} & \frac{\partial R_i^P}{\partial N_{wj}} \\ \frac{\partial R_{1,i}^N}{\partial P_j} & \frac{\partial R_{1,i}^N}{\partial N_{1j}} & \cdots & \frac{\partial R_{1,i}^N}{\partial N_{n_c j}} & \frac{\partial R_{1,i}^N}{\partial N_{wj}} \\ \vdots & \vdots & \ddots & \vdots & \vdots \\ \frac{\partial R_{n_c,i}^N}{\partial P_j} & \frac{\partial R_{n_c,i}^N}{\partial N_{1j}} & \cdots & \frac{\partial R_{n_c,i}^N}{\partial N_{n_c j}} & \frac{\partial R_{n_c,i}^N}{\partial N_{wj}} \\ \frac{\partial R_{w,i}^N}{\partial P_j} & \frac{\partial R_{w,i}^N}{\partial N_{1j}} & \cdots & \frac{\partial R_{w,i}^N}{\partial N_{n_c j}} & \frac{\partial R_{w,i}^N}{\partial N_{wj}} \end{bmatrix}, \tag{23}$$

$$\Delta X_i = \begin{bmatrix} \Delta P_i \\ \Delta N_{1,i} \\ \vdots \\ \Delta N_{n_c,i} \\ \Delta X_{w,i} \end{bmatrix}, \tag{24}$$

and

$$R_i = \begin{bmatrix} R_i^P \\ R_{1,i}^N \\ \vdots \\ R_{n_c i}^N \\ R_{w,i}^N \end{bmatrix}. \tag{25}$$

The variable change is then applied only to the fully implicit blocks. The Jacobian for Collins et al. [11] formulation considering a 1D discretization with three hydrocarbon components plus water (Fig. 2) is shown in Fig. 3. In this example, two gridblocks are treated as FI and two are treated as IMPEC.

	P	Z_1	Z_2	N_T	S_w	P	N_1	N_2	N_3	N_w	P	N_1	N_2	N_3	N_w	P	Z_1	Z_2	N_T	S_w
R^P	+	+	+	+	+															
R_1^N	+	+	+	+	+	X														
R_2^N	+	+	+	+	+	X														
R_3^N	+	+	+	+	+	X														
R_w^N	+	+	+	+	+	X														
R^P						X	X	X	X	X										
R_1^N	+	+	+		+	X	X				X									
R_2^N	+	+	+		+	X		X			X									
R_3^N	+	+	+		+	X			X		X									
R_w^N	+	+	+		+	X				X	X									
R^P											X	X	X	X	X					
R_1^N						X					X	X				+	+	+		+
R_2^N						X					X		X			+	+	+		+
R_3^N						X					X			X		+	+	+		+
R_w^N						X					X				X	+	+	+		+
R^P																+	+	+	+	+
R_1^N											X					+	+	+	+	+
R_2^N											X					+	+	+	+	+
R_3^N											X					+	+	+	+	+
R_w^N											X					+	+	+	+	+

Fig. 4. Illustration of the Jacobian obtained using the Collins et al. [11] formulation after the variable exchange from Fernandes et al. [8].

The variable change, proposed in Fernandes et al. [8], is applied to the Jacobian in Fig. 3 and results in the matrix presented in Fig. 4. The variable change is applied only to fully implicit blocks, changing the variable set from $\{P, N_k\}$ to $\{P, Z_k, N_T\}$. The new variable set is obtained by changing the derivatives with the following expressions:

$$\left(\frac{\partial R^P}{\partial P}\right)_{Z,N_T,S_w} = \left(\frac{\partial R^P}{\partial P}\right)_{N_k,N_w} + \left(\frac{\partial R^P}{\partial N_w}\right)_{P,N_k} S_w V_b \left[\xi_w \frac{\partial \phi}{\partial P} + \phi \frac{\partial \xi_w}{\partial P}\right], \tag{26}$$

$$\left(\frac{\partial R^P}{\partial Z_i}\right)_{P,Z_k\neq Z_i,N_T,S_w} = N_T \left(\left(\frac{\partial R^P}{\partial N_i}\right)_{P,N_k\neq N_i,N_w} - \left(\frac{\partial R^P}{\partial N_{n_c}}\right)_{P,N_k\neq N_{n_c},N_w}\right), \quad i = 1,\ldots,n_c-1, \tag{27}$$

$$\left(\frac{\partial R^P}{\partial N_T}\right)_{P,Z_k,S_w} = \sum_{l=1}^{n_c-1} Z_l \left(\left(\frac{\partial R^P}{\partial N_l}\right)_{P,N_k\neq N_l,N_w} - \left(\frac{\partial R^P}{\partial N_{n_c}}\right)_{P,N_k\neq N_{n_c},N_w}\right), \tag{28}$$

$$\left(\frac{\partial R^P}{\partial S_w}\right)_{P,Z_k,N_T} = V_b \xi_w \phi \left(\frac{\partial R^P}{\partial N_w}\right)_{P,N_k}, \tag{29}$$

$$\left(\frac{\partial R_j^N}{\partial P}\right)_{Z_k,N_T,S_w} = \left(\frac{\partial R_j^N}{\partial P}\right)_{N_k,N_w} + \left(\frac{\partial R_j^N}{\partial N_k}\right)_{P,N_k,} S_w V_b \left[\xi_w \frac{\partial \phi}{\partial P} + \phi \frac{\partial \xi_w}{\partial P}\right], \quad j = 1,\ldots,n_c+1 \tag{30}$$

$$\left(\frac{\partial R_j^N}{\partial Z_i}\right)_{P,Z_k\neq Z_i,N_T,S_w} = N_T \left(\left(\frac{\partial R_j^N}{\partial N_i}\right)_{P,N_k\neq N_i,N_w} - \left(\frac{\partial R_j^N}{\partial N_{n_c}}\right)_{P,N_k\neq N_{n_c},N_w}\right), \quad i = 1,\ldots,n_c-1;\ j = 1,\ldots,n_c+1, \tag{31}$$

$$\left(\frac{\partial R_j^N}{\partial N_T}\right)_{P,Z_k,S_w} = \sum_{l=1}^{n_c-1} Z_l \left(\left(\frac{\partial R_j^N}{\partial N_l}\right)_{P,N_k\neq N_l,N_w} - \left(\frac{\partial R_j^N}{\partial N_{n_c}}\right)_{P,N_k\neq N_{n_c},N_w}\right), \quad j = 1,\ldots,n_c+1, \tag{32}$$

$$\left(\frac{\partial R_j^N}{\partial S_w}\right)_{P,Z_k,N_T} = V_b \xi_w \phi \left(\frac{\partial R_j^N}{\partial N_w}\right)_{P,N_k}, \quad j = 1,\ldots,n_c+1. \tag{33}$$

The variable set change presented in Eqs. (26) through (33) are used for all Jacobian blocks that refer to a fully implicit block and results in a Jacobian with the form of the one presented in Fig. 4. In this figure, the values that are modified by the variable change are illustrated with a '+'. Notice that only the main diagonal block of FI blocks will have non-zero derivatives with respect to the total number of moles (N_T). Both advection and dispersive fluxes are not a function of extensive variables which is why the derivatives of residues with respect to N_T of the off-diagonal blocks are zero.

A Gauss elimination is then used to have only the derivative of pressure equation with respect to N_T non-zero on the main diagonal block for the fully implicit gridblocks. The resulting Jacobian structure is illustrated in Fig. 5, and the modified values are now illustrated with '+'.

	P	Z_1	Z_2	N_T	S_w	P	N_1	N_2	N_3	N_w	P	N_1	N_2	N_3	N_w	P	Z_1	Z_2	N_T	S_w
R^P	+	+	+	+	+															
R_1^N	+	+	+		+	X														
R_2^N	+	+	+		+	X														
R_3^N	+	+	+		+	X														
R_w^N	+	+	+		+	X														
R^P						X	X	X	X	X										
R_1^N	+	+	+		+	X	X				X									
R_2^N	+	+	+		+	X		X			X									
R_3^N	+	+	+		+	X			X		X									
R_w^N	+	+	+		+	X				X	X									
R^P											X	X	X	X	X					
R_1^N						X					X	X				+	+	+		+
R_2^N						X					X		X			+	+	+		+
R_3^N						X					X			X		+	+	+		+
R_w^N						X					X				X	+	+	+		+
R^P																+	+	+	+	+
R_1^N											X					+	+	+		+
R_2^N											X					+	+	+		+
R_3^N											X					+	+	+		+
R_w^N											X					+	+	+		+

Fig. 5. Illustration of the Jacobian obtained using the Collins et al. [11] after the variable exchange from Fernandes et al. [8] and elimination of the total number of moles.

	P	Z_1	Z_2	S_w	P	N_1	N_2	N_3	N_w	P	N_1	N_2	N_3	N_w	P	Z_1	Z_2	S_w
R_1^N	+	+	+	+	X													
R_2^N	+	+	+	+	X													
R_3^N	+	+	+	+	X													
R_w^N	+	+	+	+	X													
R^P					X	X	X	X	X									
R_1^N	+	+	+	+	X	X				X								
R_2^N	+	+	+	+	X		X			X								
R_3^N	+	+	+	+	X			X		X								
R_w^N	+	+	+	+	X				X	X								
R^P										X	X	X	X	X				
R_1^N					X					X	X				+	+	+	+
R_2^N					X					X		X			+	+	+	+
R_3^N					X					X			X		+	+	+	+
R_w^N					X					X				X	+	+	+	+
R_1^N										X					+	+	+	+
R_2^N										X					+	+	+	+
R_3^N										X					+	+	+	+
R_w^N										X					+	+	+	+

Fig. 6. Illustration of the reduced Jacobian after changing the FI set into an intensive set.

Due to the Jacobian's new structure, one can separate the pressure equation and solve for pressure, overall compositions, and water saturation for FI gridblocks and pressure and component moles for IMPEC gridblocks (Fig. 6). After solving these, the total number of moles for the FI gridblocks can be calculated with the pressure equation residues.

Further simplification of the linear system can be achieved if another Gauss elimination is carried on the main diagonal block of IMPEC gridblocks. The idea now is to eliminate the dependence of the pressure equation for IMPEC gridblocks with respect to the number of moles, thus making these blocks lower triangular (Fig. 7). The values of the Jacobian modified with this elimination are illustrated in Fig. 7 with a '*'.

After the above elimination, one can solve for pressure in IMPEC gridblocks first, and then use that result to calculate the number of moles (Fig. 8). Therefore, after solving the primary unknowns, $\{P, Z_i, S_w\}$ for FI and $\{P\}$ for IMPEC gridblocks, one can use this solution to calculate the secondary unknowns, $\{N_T\}$ for FI and $\{N_i\}$ for the IMPEC gridblocks.

Following the ideas of Coats [16], two switching criteria are considered. First, the use of explicit saturations is tested with a stability analysis. Second, the use of explicit compositions for each gridblock is tested using the von Neumann stability analysis. The concept of Courant number (CFL) is used in order to describe the switching criterion for explicit composition which is given by

	P	Z_1	Z_2	S_w	P	N_1	N_2	N_3	N_w	P	N_1	N_2	N_3	N_w	P	Z_1	Z_2	S_w
R_1^N	+	+	+	+	X													
R_2^N	+	+	+	+	X													
R_3^N	+	+	+	+	X													
R_w^N	+	+	+	+	X													
R^P	*	*	*	*	*					*								
R_1^N	+	+	+	+	X	X				X								
R_2^N	+	+	+	+	X		X			X								
R_3^N	+	+	+	+	X			X		X								
R_w^N	+	+	+	+	X				X	X								
R^P					*					*					*	*	*	*
R_1^N					X					X	X				+	+	+	+
R_2^N					X					X		X			+	+	+	+
R_3^N					X					X			X		+	+	+	+
R_w^N					X					X				X	+	+	+	+
R_1^N										X					+	+	+	+
R_2^N										X					+	+	+	+
R_3^N										X					+	+	+	+
R_w^N										X					+	+	+	+

Fig. 7. Illustration of the reduced Jacobian after eliminating the number of moles dependence from the pressure equation into the IMPEC blocks.

	P	Z_1	Z_2	S_w	P	P	P	Z_1	Z_2	S_w
R_1^N	+	+	+	+	X					
R_2^N	+	+	+	+	X					
R_3^N	+	+	+	+	X					
R_w^N	+	+	+	+	X					
R^P	*	*	*	*	*	*				
R^P					*	*	*	*	*	*
R_1^N						X	+	+	+	+
R_2^N						X	+	+	+	+
R_3^N						X	+	+	+	+
R_w^N						X	+	+	+	+

Fig. 8. Illustration of the final reduced Jacobian.

$$CFL = F\frac{\Delta t}{\phi V_b}. \tag{34}$$

For the explicit compositions, we use the same criterion as presented by Coats [16], as this approach is valid regardless of the number of phases present in the gridblock. In such a case, one value of F could be obtained for each component flowing, but only the highest value matters for the stability. Therefore, the value of F is computed as presented below:

$$F = \max_k\left(\frac{\sum_{j=2}^{n_p} Q_j x_{jk}\xi_j}{\sum_{j=2}^{n_p} S_j x_{jk}\xi_j}\right), \tag{35}$$

where Q_j is the total volumetric flow rate of phase j flowing out of a gridblock. For simplification purposes, the water component was not included in Eq. (35).

With the approach from Coats [16], using the explicit composition and explicit saturation criteria, two distinct CFL numbers are computed for each gridblock. If both of these CFL numbers are less than or equal to a specified number, normally the unity, the gridblock is set as IMPEC; otherwise, the gridblock is set as fully implicit. However, here the switching criterion for the explicit saturations case is obtained straight from the spectral radius of the error amplification matrix as will be presented next. A gridblock can only be considered IMPEC if both switching criteria are satisfied.

For all cases presented in the result section, the linear systems were solved by a GMRES method [37] with restart option and the left ILU(1) preconditioner customized for variable linear system structures implemented in the PETSc 3.12 version [38].

5. New generalized stability analysis for explicit saturations

In order to obtain the switching criteria for our adaptive implicit scheme, we use the von Neumann stability method. The first step is to write the equations for the saturations considering them explicitly. In this work, we use the Buckley-Leverett equations for the saturations. The 1D Buckley-Leverett equation for phase l is written as

$$\frac{\Delta V_{pi}}{\Delta t}\left(S_{l,i}^{n+1}-S_{l,i}^{n}\right)=q_{l,i-1/2}-q_{l,i+1/2}, \tag{36}$$

where

$$q_{l,i-1/2}=-\frac{k_{rl,i-1/2}}{\mu_{l,i-1/2}}T_{i-1/2}\left(P_{i}^{n+1}-P_{i-1}^{n+1}-\gamma_{l,i-\frac{1}{2}}^{n}(D_i-D_{i-1})+P_{cl,i}^{n}-P_{cl,i-1}^{n}\right), \tag{37}$$

and

$$q_{l,i+1/2}=-\frac{k_{rl,i+1/2}}{\mu_{l,i+1/2}}T_{i+1/2}\left(P_{i+1}^{n+1}-P_{i}^{n+1}-\gamma_{l,i+\frac{1}{2}}^{n}(D_{i+1}-D_i)+P_{cl,i+1}^{n}-P_{cl,i}^{n}\right). \tag{38}$$

One can write the saturation error for phase l in gridblock i as

$$\varepsilon_{l,i}=S_{l,i}-S_{l,i}^{*}, \tag{39}$$

where $S_{l,i}^{*}$ is the saturation of phase l obtained from the exact solution.

If we use Eq. (36) for the exact and approximate solutions, and subtract them, we obtain:

$$\frac{\Delta V_{pi}}{\Delta t}\left(S_{l,i}^{n+1}-S_{l,i}^{n}\right)-\frac{\Delta V_{pi}}{\Delta t}\left(S_{l,i}^{*,n+1}-S_{l,i}^{*,n}\right)=q_{l,i-1/2}-q_{l,i-1/2}^{*}-q_{l,+1/2}+q_{l,i+1/2}^{*}. \tag{40}$$

Therefore,

$$\frac{\Delta V_{pi}}{\Delta t}\left(\varepsilon_{l,i}^{n+1}-\varepsilon_{l,i}^{n}\right)=q_{l,i-1/2}-q_{l,i-1/2}^{*}-q_{l,+1/2}+q_{l,i+1/2}^{*}. \tag{41}$$

The exact rates can be approximated in terms of the approximated rates using Taylor series as

$$q_{l,i-1/2}^{*}=q_{l,i-1/2}+\sum_{\substack{j=1\\ j\neq r}}^{n_p}\frac{\partial q_{l,i-1/2}}{\partial S_{j,i-1}^{n}}\left(S_{j,i-1}^{*,n}-S_{j,i-1}^{n}\right)+\sum_{\substack{j=1\\ j\neq r}}^{n_p}\frac{\partial q_{l,i-1/2}}{\partial S_{j,i}^{n}}\left(S_{j,i}^{*,n}-S_{j,i}^{n}\right), \tag{42}$$

and

$$q_{l,i+1/2}^{*}=q_{l,i+1/2}+\sum_{\substack{j=1\\ j\neq r}}^{n_p}\frac{\partial q_{l,i+1/2}}{\partial S_{j,i+1}^{n}}\left(S_{j,i+1}^{*,n}-S_{j,i+1}^{n}\right)+\sum_{\substack{j=1\\ j\neq r}}^{n_p}\frac{\partial q_{l,i+1/2}}{\partial S_{j,i}^{n}}\left(S_{j,i}^{*,n}-S_{j,i}^{n}\right). \tag{43}$$

Hence,

$$q_{l,i-1/2}^{*}=q_{l,i-1/2}-\sum_{\substack{j=1\\ j\neq r}}^{n_p}\frac{\partial q_{l,i-1/2}}{\partial S_{j,i-1}^{n}}\varepsilon_{j,i-1}^{n}-\sum_{\substack{j=1\\ j\neq r}}^{n_p}\frac{\partial q_{l,i-1/2}}{\partial S_{j,i}^{n}}\varepsilon_{j,i}^{n}, \tag{44}$$

and

$$q_{l,i+1/2}^{*}=q_{l,i+1/2}-\sum_{\substack{j=1\\ j\neq r}}^{n_p}\frac{\partial q_{l,i+1/2}}{\partial S_{j,i+1}^{n}}\varepsilon_{j,i+1}^{n}-\sum_{\substack{j=1\\ j\neq r}}^{n_p}\frac{\partial q_{l,i+1/2}}{\partial S_{j,i}^{n}}\varepsilon_{j,i}^{n}, \tag{45}$$

where

$$\frac{\partial q_{l,i-1/2}}{\partial S_{j,k}^{n}}=-\frac{T_{i-1/2}}{\mu_{l,i-1/2}}\left[-\frac{\partial k_{rl,i-1/2}^{n}}{\partial S_{j,k}^{n}}\Delta\Phi_{l,i-1/2}+k_{rl,i-1/2}^{n}\left(\frac{\partial P_{cl,i}^{n}}{\partial S_{j,k}^{n}}-\frac{\partial P_{cl,i-1}^{n}}{\partial S_{j,k}^{n}}\right)\right], \tag{46}$$

and

$$\frac{\partial q_{l,i+1/2}}{\partial S_{j,k}^{n}}=-\frac{T_{i+1/2}}{\mu_{l,i+1/2}}\left[\frac{\partial k_{rl,i+1/2}^{n}}{\partial S_{j,k}^{n}}\Delta\Phi_{l,i+1/2}+k_{rl,i+1/2}^{n}\left(\frac{\partial P_{cl,i+1}^{n}}{\partial S_{j,k}^{n}}-\frac{\partial P_{cl,i}^{n}}{\partial S_{j,k}^{n}}\right)\right], \tag{47}$$

where in the above equation k denotes i, $i+1$, or $i-1$, and the potential differences are computed as

$$\Delta\Phi_{l,i+1/2}=P_{i+1}^{n+1}-P_{i}^{n+1}-\gamma_{i+1/2}^{n+1}(D_{i+1}-D_i)+P_{cl,i+1}^{n}-P_{cl,i}^{n}, \tag{48}$$

and

$$\Delta\Phi_{l,i-1/2} = P_{i-1}^{n+1} - P_i^{n+1} - \gamma_{i-1/2}^{n+1}(D_{i-1} - D_i) + P_{cl,i-1}^n - P_{cl,i}^n. \tag{49}$$

Substituting the above results into Eq. (41), we obtain

$$\frac{\Delta V_{pi}}{\Delta t}\left(\varepsilon_{l,i}^{n+1} - \varepsilon_{l,i}^n\right) = \sum_{\substack{j=1\\ j\neq r}}^{n_p} \frac{\partial q_{l,i-1/2}}{\partial S_{j,i-1}^n}\varepsilon_{j,i-1}^n + \sum_{\substack{j=1\\ j\neq r}}^{n_p} \frac{\partial q_{l,i-1/2}}{\partial S_{j,i}^n}\varepsilon_{j,i}^n - \sum_{\substack{j=1\\ j\neq r}}^{n_p} \frac{\partial q_{l,i+1/2}}{\partial S_{j,i+1}^n}\varepsilon_{j,i+1}^n - \sum_{\substack{j=1\\ j\neq r}}^{n_p} \frac{\partial q_{l,i+1/2}}{\partial S_{j,i}^n}\varepsilon_{j,i}^n. \tag{50}$$

Hence,

$$\frac{\Delta V_{pi}}{\Delta t}\left(\varepsilon_{l,i}^{n+1} - \varepsilon_{l,i}^n\right) = \sum_{\substack{j=1\\ j\neq r}}^{n_p} \left(\frac{\partial q_{l,i-1/2}}{\partial S_{j,i-1}^n}\right)\varepsilon_{j,i-1}^n + \sum_{\substack{j=1\\ j\neq r}}^{n_p} \left(\frac{\partial q_{l,i-1/2}}{\partial S_{j,i}^n} - \frac{\partial q_{l,i+1/2}}{\partial S_{j,i}^n}\right)\varepsilon_{j,i}^n + \sum_{\substack{j=1\\ j\neq r}}^{n_p} \left(-\frac{\partial q_{l,i+1/2}}{\partial S_{j,i+1}^n}\right)\varepsilon_{j,i+1}^n. \tag{51}$$

Equation (51) can be rewritten as

$$\varepsilon_{l,i}^{n+1} - \varepsilon_{l,i}^n = \sum_{\substack{j=1\\ j\neq r}}^{n_p} c_{lj}\varepsilon_{j,i-1}^n - \sum_{\substack{j=1\\ j\neq r}}^{n_p} b_{lj}\varepsilon_{j,i}^n + \sum_{\substack{j=1\\ j\neq r}}^{n_p} a_{lj}\varepsilon_{j,i+1}^n, \tag{52}$$

where

$$a_{lj} = -\frac{\Delta t}{\Delta V_{pi}}\frac{\partial q_{l,i+1/2}}{\partial S_{j,i+1}^n}, \tag{53}$$

$$b_{lj} = \frac{\Delta t}{\Delta V_{pi}}\left(\frac{\partial q_{l,i+1/2}}{\partial S_{j,i}^n} - \frac{\partial q_{l,i-1/2}}{\partial S_{j,i}^n}\right), \tag{54}$$

and

$$c_{lj} = \frac{\Delta t}{\Delta V_{pi}}\frac{\partial q_{l,i-1/2}}{\partial S_{j,i-1}^n}. \tag{55}$$

Let $r = n_p$, $h = l$, and $g = j$:

$$\varepsilon_{h,i}^{n+1} - \varepsilon_{h,i}^n = \sum_{g=1}^{n_p-1} c_{hg}\varepsilon_{g,i-1}^n - \sum_{g=1}^{n_p-1} b_{hg}\varepsilon_{g,i}^n + \sum_{g=1}^{n_p-1} a_{hg}\varepsilon_{g,i+1}^n, \quad h = 1,\ldots,n_p-1. \tag{56}$$

We assume the error function as a periodic function of the form:

$$\varepsilon_{h,i}^n = \lambda_h^n e^{\hat{i}i\beta_h}, \quad h = 1,\ldots,n_p-1, \tag{57}$$

with

$$\lambda_h = \frac{\varepsilon_{h,i}^{n+1}}{\varepsilon_{h,i}^n}, \quad h = 1,\ldots,n_p-1. \tag{58}$$

Substituting Eq. (57) into Eq. (56), we obtain

$$\lambda_h^{n+1}e^{\hat{i}i\beta_h} - \lambda_h^n e^{\hat{i}i\beta_h} = \sum_{g=1}^{n_p-1} c_{hg}\lambda_g^n e^{(\hat{i}-1)i\beta_g} - \sum_{g=1}^{n_p-1} b_{hg}\lambda_g^n e^{\hat{i}i\beta_g} + \sum_{g=1}^{n_p-1} a_{hg}\lambda_g^n e^{(\hat{i}+1)i\beta_g}, \quad h = 1,\ldots,n_p-1, \tag{59}$$

or

$$\lambda_h^{n+1}e^{\hat{i}i\beta_h} - \lambda_h^n e^{\hat{i}i\beta_h} = \sum_{g=1}^{n_p-1} c_{hg}\lambda_g^n e^{-i\beta_g}e^{\hat{i}i\beta_g} - \sum_{g=1}^{n_p-1} b_{hg}\lambda_g^n e^{\hat{i}i\beta_g} + \sum_{g=1}^{n_p-1} a_{hg}\lambda_g^n e^{i\beta_g}e^{\hat{i}i\beta_g}, \quad h = 1,\ldots,n_p-1. \tag{60}$$

Hence,

$$\lambda_h^{n+1}e^{\hat{i}i\beta_h} = \sum_{g=1}^{n_p-1}\left(a_{hg}e^{i\beta_g} + \delta_{hg} - b_{hg} + c_{hg}e^{-i\beta_g}\right)\lambda_g^n e^{\hat{i}i\beta_g}, \quad h = 1,\ldots,n_p-1, \tag{61}$$

with

$$\delta_{hg} = \begin{cases} 1, & \text{for } h = g \\ 0, & \text{for } h \neq g. \end{cases} \tag{62}$$

Therefore, writing Eq. (61) in terms of the error again we obtain

$$\varepsilon_{h,i}^{n+1} = \sum_{g=1}^{n_p-1} \left(a_{hg} e^{i\beta_g} + \delta_{hg} - b_{hg} + c_{hg} e^{-i\beta_g}\right) \varepsilon_{g,i}^{n}, \quad h = 1, \ldots, n_p - 1. \tag{63}$$

Applying the trigonometric identities to the exponentials in Eq. (63), we obtain

$$\varepsilon_{h,i}^{n+1} = \sum_{g=1}^{n_p-1} \left(a_{hg}\left(\cos(\beta_g) + i\sin(\beta_g)\right) + \delta_{hg} - b_{hg} + c_{hg}\left(\cos(\beta_g) - i\sin(\beta_g)\right)\right) \varepsilon_{g,i}^{n}, \quad h = 1, \ldots, n_p - 1. \tag{64}$$

The error equations can then be written in a matrix form as:

$$\vec{\varepsilon}_i^{n+1} = \boldsymbol{T}\vec{\varepsilon}_i^{n}, \tag{65}$$

where $\boldsymbol{T}$ is the amplification matrix, written as

$$\boldsymbol{T} = \begin{bmatrix} 1 - d_{11} & -d_{12} & \cdots & -d_{1(n_p-1)} \\ -d_{21} & 1 - d_{22} & \cdots & -d_{2(n_p-1)} \\ \vdots & \vdots & \ddots & \vdots \\ -d_{(n_p-1)1} & -d_{(n_p-1)2} & \cdots & 1 - d_{(n_p-1)(n_p-1)} \end{bmatrix}. \tag{66}$$

The coefficients of the amplification matrix are given by

$$d_{rs} = -(a_{rs} + c_{rs})\cos(\beta_s) + b_{rs} - (a_{rs} - c_{rs})i\sin(\beta_s), \quad r = 1, \ldots, n_p - 1; s = 1, \ldots, n_p - 1. \tag{67}$$

For a two-phase flow, the maximum eigenvalue is obtained when the following conditions are satisfied:

$$\cos(\beta_s) = -1, \tag{68}$$

and

$$\sin(\beta_s) = 0. \tag{69}$$

Following the same assumption as Coats [16], we assume that Eqs. (68) and (69) hold for any multiphase case. Therefore, Eq. (67) can be rewritten as

$$d_{rs} = a_{rs} + b_{rs} + c_{rs}, \quad r = 1, \ldots, n_p - 1; s = 1, \ldots, n_p - 1. \tag{70}$$

The coefficients, for a 1D fluid flow are computed as

$$\begin{aligned} d_{rs} = {} & \frac{\Delta t}{\Delta V_{pi}} \frac{T_{i+\frac{1}{2}}}{\mu_{r,i+\frac{1}{2}}} \left[\frac{\partial k_{rr,i+\frac{1}{2}}^{n}}{\partial S_{s,i+1}^{n}} \Delta\Phi_{r,i+\frac{1}{2}} + k_{rr,i+\frac{1}{2}}^{n} \left(\frac{\partial P_{cr,i+1}^{n}}{\partial S_{s,i+1}^{n}} \right) \right] \\ & - \frac{\Delta t}{\Delta V_{pi}} \frac{T_{i+\frac{1}{2}}}{\mu_{r,i+\frac{1}{2}}} \left[\frac{\partial k_{rr,i+\frac{1}{2}}^{n}}{\partial S_{s,i}^{n}} \Delta\Phi_{r,i+\frac{1}{2}} + k_{rr,i+\frac{1}{2}}^{n} \left(-\frac{\partial P_{cr,i}^{n}}{\partial S_{s,i}^{n}} \right) \right] \\ & + \frac{\Delta t}{\Delta V_{pi}} \frac{T_{i-\frac{1}{2}}}{\mu_{r,i-\frac{1}{2}}} \left[-\frac{\partial k_{rr,i-\frac{1}{2}}^{n}}{\partial S_{s,i}^{n}} \Delta\Phi_{r,i-\frac{1}{2}} + k_{rr,i-\frac{1}{2}}^{n} \left(\frac{\partial P_{cr,i}^{n}}{\partial S_{s,i}^{n}} \right) \right] \\ & - \frac{\Delta t}{\Delta V_{pi}} \frac{T_{i-\frac{1}{2}}}{\mu_{r,i-\frac{1}{2}}} \left[-\frac{\partial k_{rr,i-\frac{1}{2}}^{n}}{\partial S_{s,i-1}^{n}} \Delta\Phi_{r,i-\frac{1}{2}} + k_{rr,i-\frac{1}{2}}^{n} \left(-\frac{\partial P_{cr,i-1}^{n}}{\partial S_{s,i-1}^{n}} \right) \right], \quad r = 1, \ldots, n_p - 1; s = 1, \ldots, n_p - 1, \end{aligned} \tag{71}$$

or

$$\begin{aligned} d_{rs} = {} & -\frac{\Delta t}{\Delta V_{pi}} \left\{ \frac{T_{i+\frac{1}{2}}}{\mu_{r,i+\frac{1}{2}}} \left[\left(\frac{\partial k_{rr,i+\frac{1}{2}}^{n}}{\partial S_{s,i}^{n}} - \frac{\partial k_{rr,i+\frac{1}{2}}^{n}}{\partial S_{s,i+1}^{n}} \right) \Delta\Phi_{r,i+\frac{1}{2}} - k_{rr,i+\frac{1}{2}}^{n} \left(\frac{\partial P_{cr,i}^{n}}{\partial S_{s,i}^{n}} + \frac{\partial P_{cr,i+1}^{n}}{\partial S_{s,i+1}^{n}} \right) \right] \right. \\ & \left. + \frac{T_{i-\frac{1}{2}}}{\mu_{r,i-\frac{1}{2}}} \left[\left(\frac{\partial k_{rr,i-\frac{1}{2}}^{n}}{\partial S_{s,i}^{n}} - \frac{\partial k_{rr,i-\frac{1}{2}}^{n}}{\partial S_{s,i-1}^{n}} \right) \Delta\Phi_{r,i-\frac{1}{2}} - k_{rr,i-\frac{1}{2}}^{n} \left(\frac{\partial P_{cr,i-1}^{n}}{\partial S_{s,i-1}^{n}} + \frac{\partial P_{cr,i}^{n}}{\partial S_{s,i}^{n}} \right) \right] \right\}, \\ & r = 1, \ldots, n_p - 1; s = 1, \ldots, n_p - 1. \end{aligned} \tag{72}$$

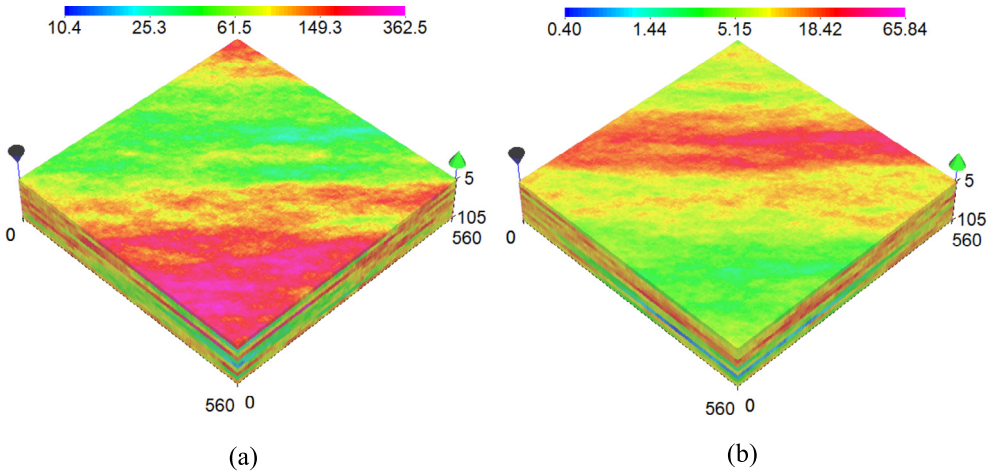

Fig. 9. Absolute permeability fields (mD) for Case 1. (a) *X* and *Y* directions and (b) *Z* direction. (For interpretation of the colors in the figure(s), the reader is referred to the web version of this article.)

Equation (72) can be generalized, following a similar approach to Coats [16], obtaining

$$d_{rs} = -\frac{\Delta t}{\Delta V_{pi}} \sum_{m=1}^{n_{faces}} \frac{T_m}{\mu_{r,m}} \left[\left(\frac{\partial k^n_{rr,m}}{\partial S^n_{s,i}} - \frac{\partial k^n_{rr,m}}{\partial S^n_{s,M}} \right) \Delta\Phi_{r,m} - k^n_{rr,m} \left(\frac{\partial P^n_{cr,i}}{\partial S^n_{s,i}} + \frac{\partial P^n_{cr,M}}{\partial S^n_{s,M}} \right) \right], \tag{73}$$

$$r = 1, \ldots, n_p - 1; s = 1, \ldots, n_p - 1.$$

In Eq. (73), n_{faces} denotes the total number of interfaces of each gridblock. The eigenvalues for the amplification matrix can be computed as

$$\det(\boldsymbol{T} - \lambda \boldsymbol{I}) = 0. \tag{74}$$

The switching criterion is based on the computation of the spectral radius for the matrix T. The spectral radius is computed as

$$\rho = \max_i |\lambda_i|. \tag{75}$$

The spectral radius for the amplification matrix is computed using the Power's iteration. If the spectral radius is lower than 1, than the block is selected as IMPEC, otherwise the block is selected as FI.

6. Results and discussion

Four case studies are presented for testing and validating the adaptive implicit method developed and implemented in this work. The first two cases involve gas injection, while the last two cases consider a CO_2 flooding. The first case investigates the effects of dispersion on the numerical performance of the formulations presented in this work. Only three phases are considered for this case. The second case considers gas flooding in a heterogeneous reservoir with complex geometry discretized using inactive cells. For this case, we compare the performance of the new AIM presented in this work with the AIM from Collins et al. [11] and the FI counterparts. The goal is to compare the performance of these approaches for complex reservoirs. The third case study considers a CO_2 flooding in an areal heterogeneous reservoir with the flow of four phases. Finally, the fourth case extends the third case to a three-dimensional reservoir with complex geometry. The two first cases consider three phase flow and can safely use the switching criteria from Coats [16] for the adaptive implicit approaches. As for the last two cases, we use the switching criteria developed in this work for the adaptive implicit approaches. The results are compared in terms of the production rates, time-step profile, property fields, CPU time, and Newton iterations. The Collins et al. formulation [11] using the FI and AIM versions is compared with the PZS-FI [8] and the PZS-AIM version developed in this work.

A gas/solvent flood is presented in Case 1. Physical dispersion is considered but molecular diffusion is set to zero, as it would be negligible when compared to the physical dispersion. Two wells are completed with one injector operating at constant surface flow rate and one producer operating at constant bottom hole pressure. The reservoir pressure allows for the formation of free gas initially in the reservoir. The formation is discretized with a $160 \times 160 \times 10$ grid (256,000 gridblocks). The heterogeneous permeability field in *X* and *Y* directions is presented in Fig. 9a and the permeability field in *Z* direction is presented in Fig. 9b.

The reservoir data is presented in Table 1. The relative permeability model is based on the Stone II [39], which the parameters are shown in Table 2. The simulation is run for up to 1,000 days (about 0.822 PVI). Six components are used

Table 1
Reservoir data for Case 1.

Simulation parameters	Value
Reservoir data	
Grid	$160 \times 160 \times 10$ (256,000 active)
Number of wells	2 (1 injector / 1 producer)
Length, width, and thickness	170.69 m, 170.69 m, and 30.48 m
Porosity	0.35
Initial water saturation	0.3
Initial pressure	10.34 MPa
Formation temperature	344.26 K
Tortuosity	1.0
Longitudinal dispersivity (W/O/G)	4.74 m, 4.74 m, and 4.74 m
Transversal dispersivity (W/O/G)	0.474 m, 0.474 m, and 0.474 m
Gas injection rate	28,316 m^3/d
Producer's bottom hole pressure	8.96 MPa
Reservoir's initial composition (C_1, C_3, C_6, C_{10}, C_{15}, and C_{20})	0.5, 0.03, 0.07, 0.2, 0.15, and 0.05
Injection fluid composition (C_1, C_3, C_6, C_{10}, C_{15}, and C_{20})	0.77, 0.2, 0.01, 0.01, 0.005, and 0.005
Run data	
Simulation time (days)	1,000
Simulation time (pore volumes)	0.822

Table 2
Relative permeability data for Case 1.

Property	Value
Model	Stone II
End point relative permeabilities (k_{rw}, k_{ro}, k_{rg})	0.4, 0.9, and 0.9
Exponents (e_w, e_{ow}, e_{og}, e_g)	3.0, 2.0, 2.0, and 2.0
Residual saturations (S_{wr}, S_{owr}, S_{ogr}, S_{gr})	0.3, 0.1, 0.1, and 0.0

Table 3
Pseudo-component data for Case 1.

Component	P_c (psi)	T_c (^{o}R)	V_c (ft^3/lb-mol)	M_w (lb/lb-mol)	ω
C_1	667.8	343.0	1.6	16.0	0.013
C_3	616.3	665.7	3.2	44.1	0.152
C_6	436.9	913.4	5.9	86.2	0.301
C_{10}	304.0	1,111.8	10.1	142.3	0.488
C_{15}	200.0	1,270.0	16.7	206.0	0.650
C_{20}	162.0	1,380.0	21.5	282.0	0.850
Binary interaction coefficients					
C_1/C_{15}			0.05		
C_1/C_{20}			0.05		
C_3/C_{15}			0.005		
C_3/C_{20}			0.005		

and the properties of each component are given in Table 3, which are based on the model presented by Killough and Kossack [40].

For this case, results without the dispersion model are presented first, because it is intended to see the effects of the dispersion in the computational performance of the formulations.

Oil and gas production rates, considering no physical dispersion, are compared in Fig. 10. From this figure, it can be observed that, as expected, similar results are obtained for all the approaches tested. The small difference in the production curves is a result of numerical dispersion, caused by the larger time-step size used by the FI and AIM approaches. The time-step profiles presented in Fig. 11 show how larger the time-step for the FI/AIM approaches can be when compared to that of the IMPEC approach. It is important to mention that the AIM is able to maintain the time-step size as large as the one of the FI approaches. A maximum time-step size of 20 days was used for the FI and AIM approaches.

The gas saturation field at 1,000 days of simulation is presented in Fig. 12. From this figure, it can be observed a similar trend between the fields obtained with all the different approaches. This confirms that all different approaches provided similar physical solution.

The implicitness field at 1,000 days of simulation for the two AIM are presented in Fig. 13. From this figure, it can be observed that more than half of the gridblocks in the reservoir are implicit at this time. It should also be noted that most of the implicit blocks are in the upper part of the reservoir, which are rich in gas phase. Such behavior is expected since

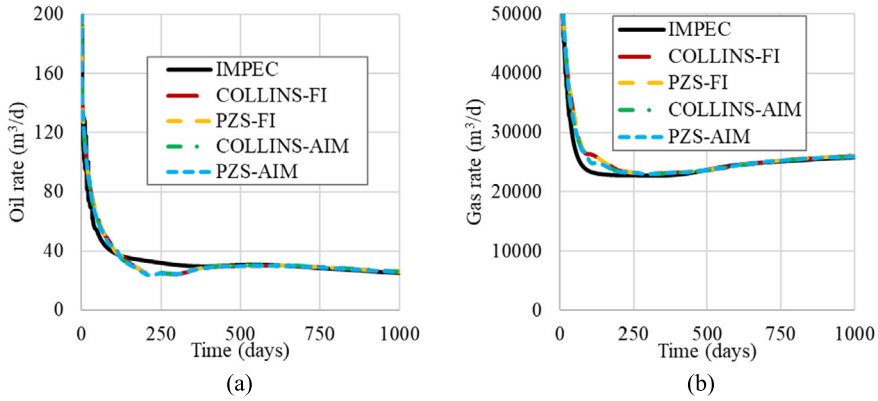

Fig. 10. Comparison of the production rates for Case 1 without dispersion. (a) Oil and (b) gas.

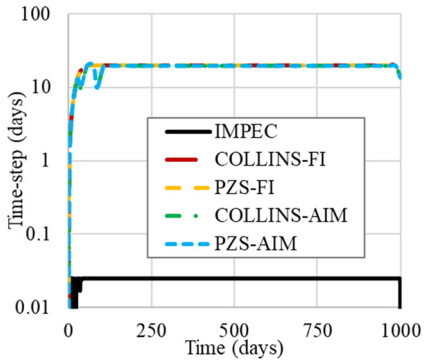

Fig. 11. Comparison of the time-step profile for Case 1 without dispersion.

Table 4
CPU time and numerical performance for Case 1 without dispersion.

Formulation	Normalized CPU time	Solver CPU time (%)	Total number of time-steps	Total number of Newton iterations	Total number of solver iterations
IMPEC	72.33	3.72	40,779	–	634,239
COLLINS-FI	1.64	79.22	67	82	7,715
PZS-FI	**1.0** (0.72 h)	65.71	67	82	7,723
COLLINS-AIM	2.20	80.45	68	106	10,240
PZS-AIM	1.85	75.34	68	106	10,460

the gas injected will preferentially flow through the upper part due to its lighter density and the higher gas mobility in the region. Therefore, the higher implicitness is actually following the regions where the velocities are higher.

The normalized CPU time and other numerical results for each approach are presented in Table 4. The approach with the best computational performance for this case was the FI version of PZS, followed by the FI version from Collins with an overhead of 64%. Between the two AIM approaches, the PZS-AIM was the fastest, with an overhead of 85% when compared to its FI counter-part. However, the IMPEC approach was considerably slower. The fact that the AIM approaches were slower than their FI counterparts for this case can be explained by the high implicitness degree in this case. For the AIM, since the linear system's structure is constantly changing, the ILU preconditioner's fill-in structure has to be recalculated frequently, unlike the FI which requires only one computation of the fill-in structure. Another factor causing overhead is the switching criteria calculation and the more complex code framework.

In Fig. 14, we compare the implicitness fraction and cumulative CPU time profiles for different sizes of the maximum time-step for the PZS-FI and PZS-AIM. Three different sizes of the maximum time-step sizes were used: 1, 5, and 20 days. One can observe that as the implicitness reduces, the AIM CPU time reduces and, at some point, becomes more advantageous than the FI. For this case study, it would appear that the implicitness fraction should be less than 0.45 in order for the AIM be more efficient than the FI. This condition is only met when the maximum time-step size is 1 day. Additionally, in Fig. 14d, two sudden increases in the CPU time for the AIM can be observed. These jumps are caused by two time-step cuts, caused by fail in convergence.

Next, the results considering dispersion are presented. Herein, not much difference was observed in the physical results considering dispersion. The production rates for the IMPEC approach with and without dispersion are presented in Fig. 15.

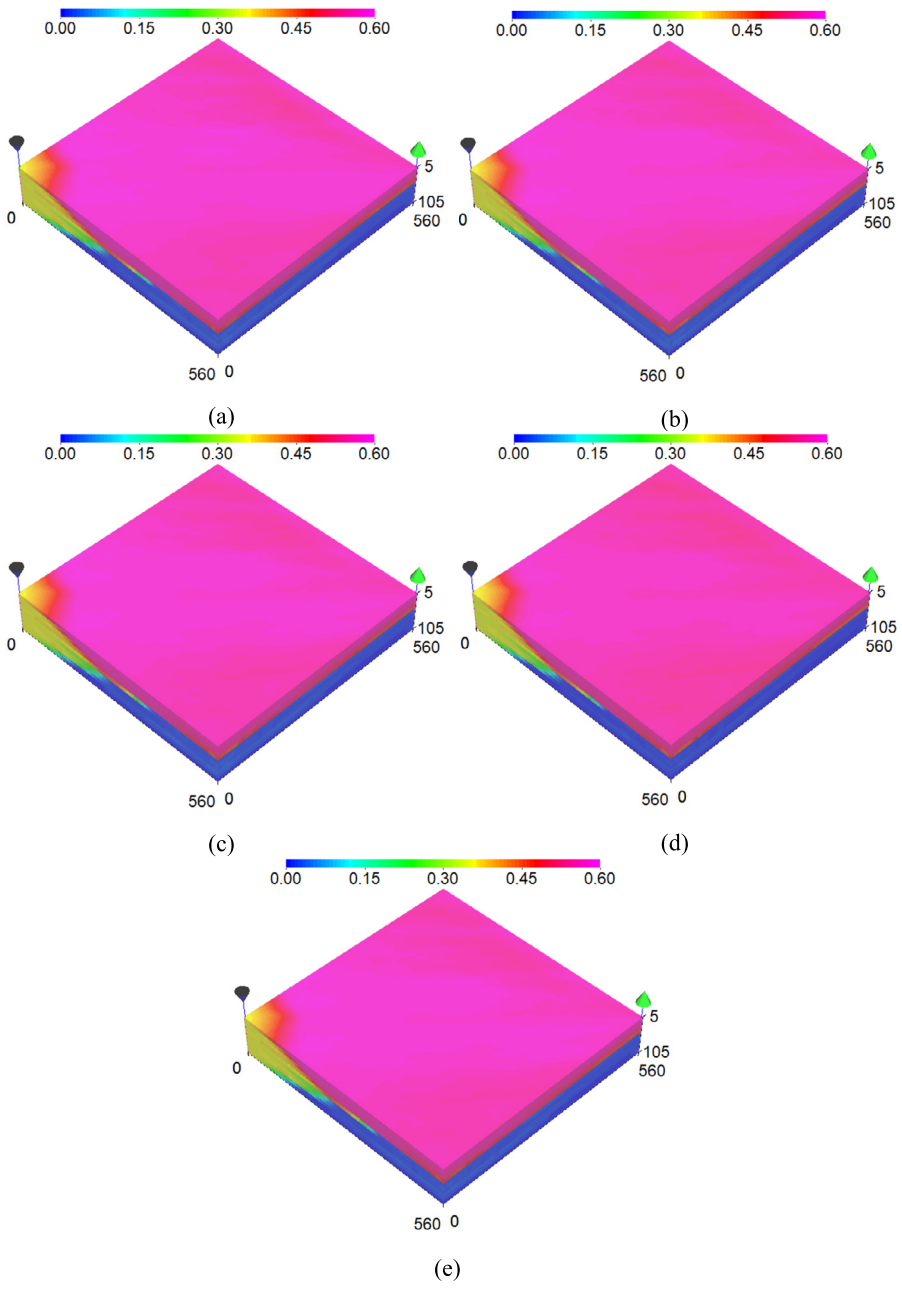

Fig. 12. Comparison of the gas saturation field at 1,000 days for Case 1 without dispersion. (a) IMPEC; (b) COLLINS-FI; (c) PZS-FI; (d) COLLINS-AIM; and (e) PZS-AIM.

In this figure, a zoom was performed for a better observation of the effects of dispersion in the production curves. Although not many changes are observed for the rates, the effects on the numerical performance of simulation are considerable, as it will be shown later.

A comparison of the oil and gas production rates with dispersion is presented in Fig. 16, where it can be observed similar production curves obtained with all the formulations.

The time-step profile is presented in Fig. 17, where it can be observed that the implicit approaches still kept a similar time-step to the case without dispersion, while the IMPEC formulation reduced the time-step size (to obtain a stable solution) considerably. This reduction in the time-step size for the IMPEC approach significantly reduced its performance.

The gas saturation field at 1,000 days of simulation is presented in Fig. 18. From this figure, it can be observed a good agreement between the fields obtained with all approaches. Once again, this result is expected as the different approaches are not supposed to change the physical solution.

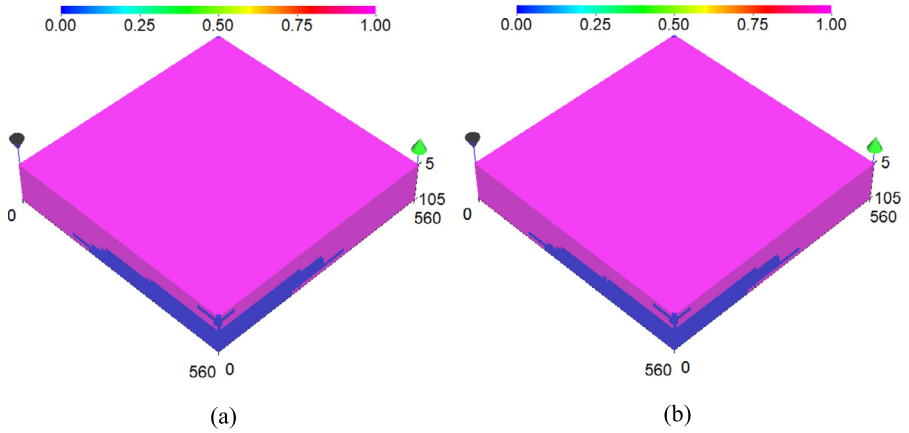

Fig. 13. Comparison of the implicitness field at 1,000 days for Case 1 without dispersion. (a) COLLINS-AIM and (b) PZS-AIM.

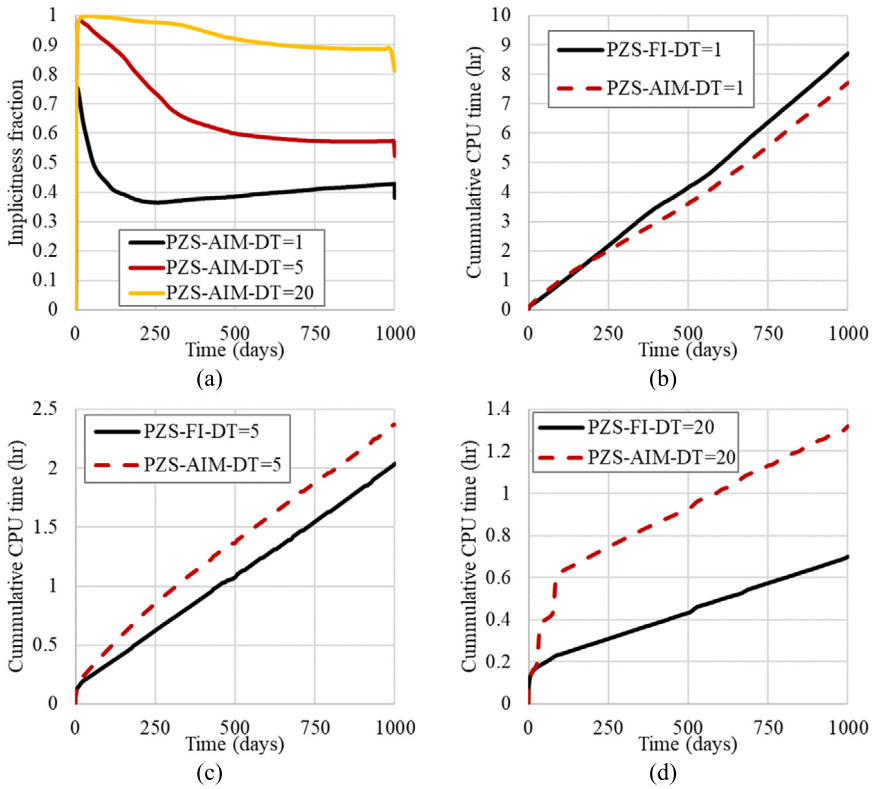

Fig. 14. Comparison of the implicitness fraction and cumulative CPU time for different time-step sizes for Case 1 without dispersion for the PZS-FI and PZS-AIM. (a) Comparison of implicitness fraction for the PZS-AIM; (b) CPU time for 1 day; (c) CPU time for 5 days; and (d) CPU time for 20 days.

The implicitness fields for the two AIM approaches at 1,000 days of simulation for are presented in Fig. 19. It can be observed that the implicitness fronts are quite similar to the ones presented in Fig. 13.

The normalized CPU time and other numerical results for each approach are presented in Table 5. From this table, it can be observed that FI and AIM approaches had a computational performance similar to the case without dispersion. However, the IMPEC approach was significantly slower than the case without dispersion. The AIM approaches required more Newton iterations, which may be a cause to the worse performance when compared the FI approaches.

Case 2 considers a gas flood in an irregular reservoir modeled with inactive cells. Forty-nine wells are considered with 25 gas injecting wells at constant rate and 24 producer wells controlled with constant bottom hole pressure. The permeability field in X and Y directions is presented in Fig. 20a and in Z direction is presented in Fig. 20b. The porosity field is shown in Fig. 21a. The reservoir's relative roof depth is presented in Fig. 21b.

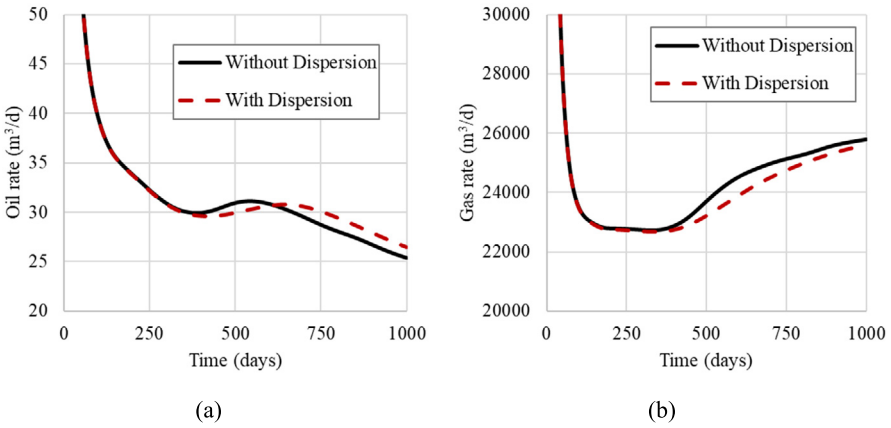

Fig. 15. Comparison of the production rates for IMPEC with and without dispersion for Case 1. (a) Oil and (b) gas.

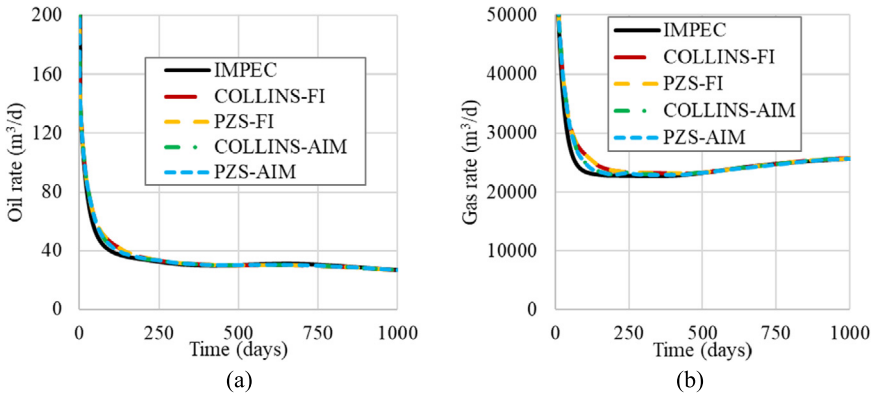

Fig. 16. Production rates for Case 1 with dispersion. (a) Oil and (b) gas.

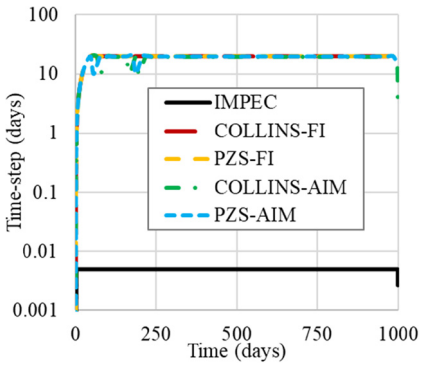

Fig. 17. Time-step profile for Case 1 with dispersion.

Table 5
CPU time and numerical performance for Case 1 with dispersion.

Formulation	Normalized CPU time	Solver CPU time (%)	Total number of time-steps	Total number of Newton iterations	Total number of solver iterations
IMPEC	200.30	1.84	200,008	–	1,160,728
COLLINS-FI	1.63	78.70	67	142	13,642
PZS-FI	**1.0** (1.26 h)	65.85	67	145	13,909
COLLINS-AIM	2.15	80.73	69	190	18,959
PZS-AIM	1.67	75.57	68	184	18,336

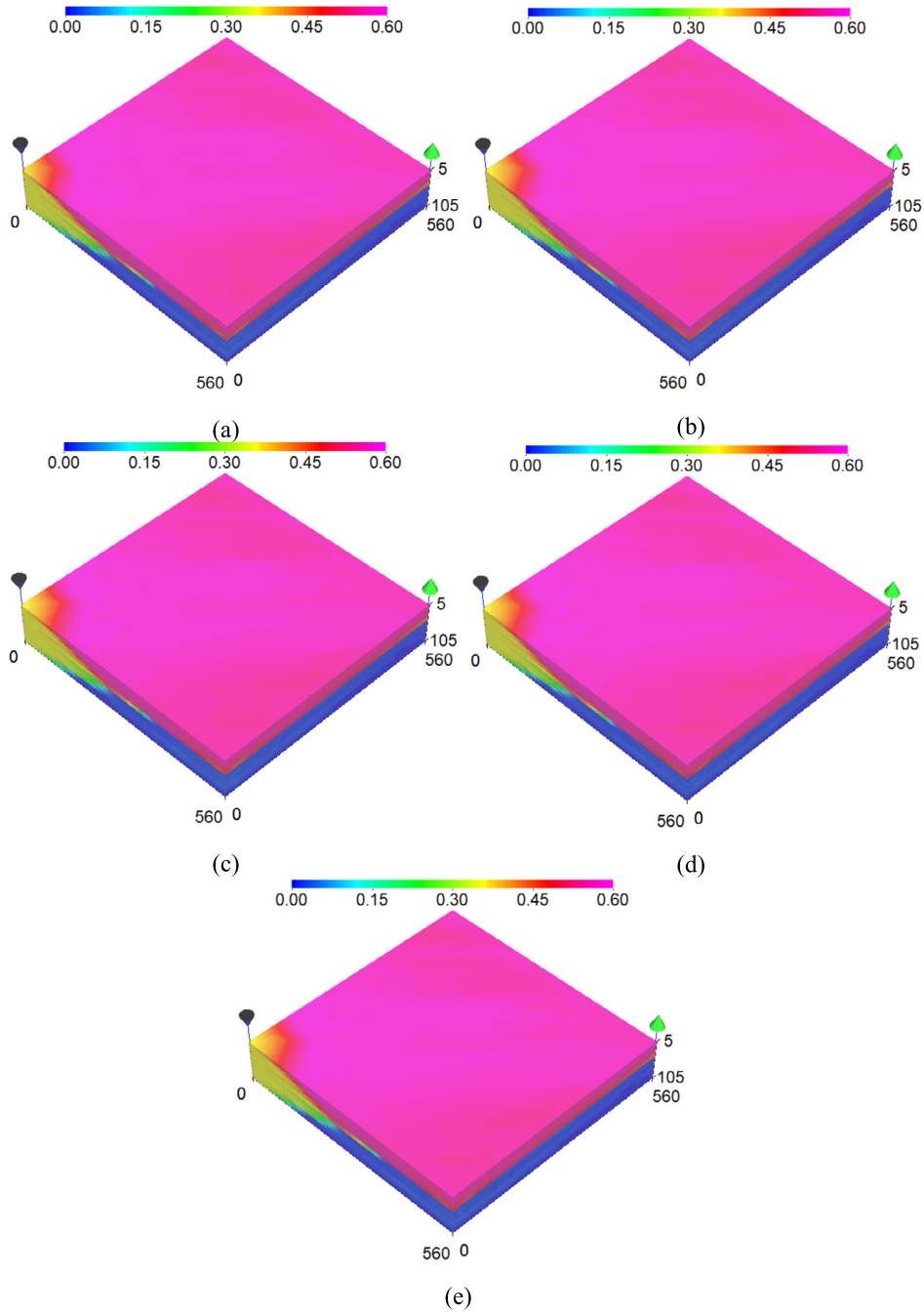

Fig. 18. Gas saturation field at 1,000 days for Case 1 with dispersion. (a) IMPEC; (b) COLLINS-FI; (c) PZS-FI; (d) COLLINS-AIM; and (e) PZS-AIM.

The reservoir data are presented in Table 6. The relative permeability model used for this case is the Stone II [39]. Data for the relative permeabilities used in this case are presented in Table 7. The simulation is run up to 2,190 days (about 1.477 PVI). Three hydrocarbon components are considered and the properties for each component are given in Table 8.

The benchmark does not consider the IMPEC approach.

A comparison of the oil and gas production rates is presented in Fig. 22. From this figure, it can be observed a match of the production rates for the different approaches.

The time-step profile is presented in Fig. 23. From this figure, it can be observed some oscillatory behavior in the time-step profile. However, in average, the PZS-AIM seems to present a higher time-step size than the COLLINS-AIM.

The gas saturation field at 2,000 days of simulation is presented in Fig. 24. From this figure, it can be observed that the gas fields are very similar for all approaches.

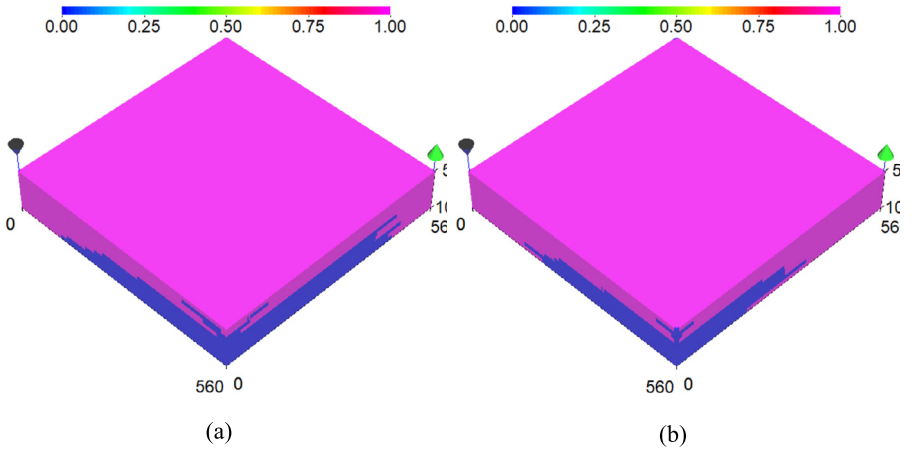

Fig. 19. Comparison of the implicitness field at 1,000 days for Case 1 with dispersion. (a) COLLINS-AIM and (b) PZS-AIM.

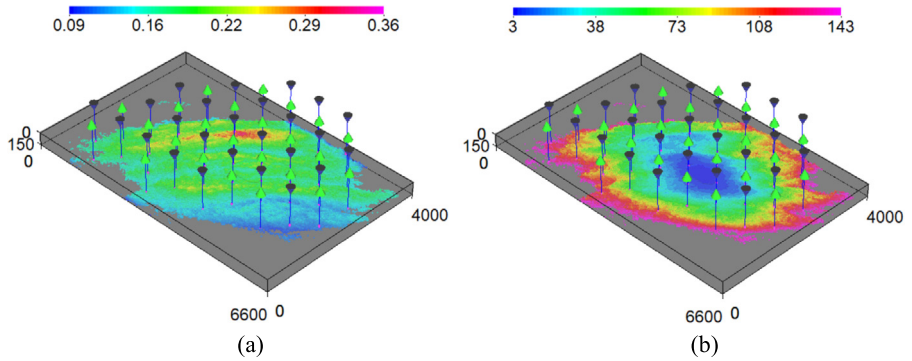

Fig. 20. Absolute permeability fields (mD) for Case 2. (a) X and Y directions and (b) Z direction.

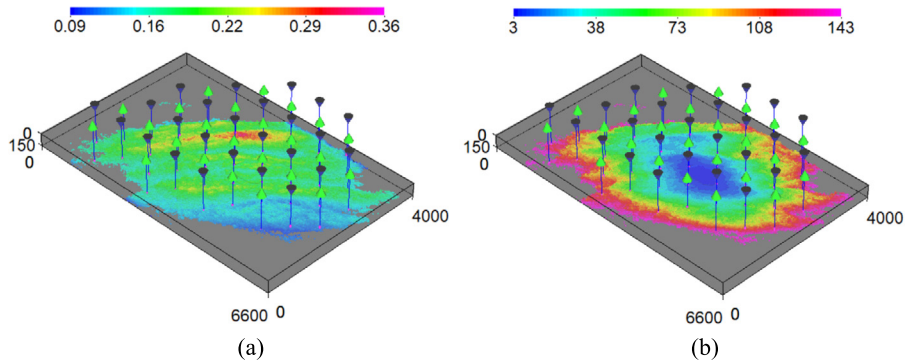

Fig. 21. Porosity field and depth for Case 2. (a) Porosity and (b) depth.

The implicitness field at 2,000 days for the two AIM approaches are presented in Fig. 25. Despite many implicit blocks are seen in this figure, it should be mentioned that less implicitness is observed in the lower parts of the reservoir, as the gas will flow mainly through the shallower parts of the reservoir.

The normalized CPU time and other numerical results for the approaches tested are presented in Table 9. It can be observed that the best performance was obtained by the AIM-PZS. The COLLINS-AIM was the second-best approach with a 17% overhead. The PZS-FI presented an overhead of 25%.

The third case study considers a 2D reservoir with heterogeneous permeabilities in the X and Y directions. The permeability field is presented in Fig. 26. Two wells are completed: one injector operating at constant bottom hole pressure and one producer operating at constant bottom hole pressure. The reservoir is discretized with a $20 \times 40 \times 1$ grid. This is a synthetic case based on the case presented by Okuno [41] using the Bob Slaughter Block (BSB) West Texas oil [42].

Table 6
Reservoir data for Case 2.

Simulation parameters	Value
Reservoir data	
Grid	$200 \times 400 \times 25$ (465,816 active)
Number of Wells	49 (25 injectors / 24 producers)
Length, width, and thickness	1,219.2 m, 2,438.4 m, and 45.72 m
Initial water saturation	0.17
Initial pressure	20.68 MPa
Formation temperature	303.15 K
Gas injection rate	86,366 m^3/d
Producer's bottom hole pressure	20.68 MPa
Reservoir's initial composition (C_1, C_3, and C_{10})	0.1, 0.19, and 0.8
Injection fluid composition (C_1, C_3, and C_{10})	0.95, 0.05, and 0.0
Run data	
Simulation time (days)	2,190
Simulation time (pore volumes)	1.477

Table 7
Relative permeability data for Case 2.

Property	Value
Model	Stone II
End point relative permeabilities (k_{rw}, k_{ro}, k_{rg})	0.9, 1.0, and 1.0
Exponents (e_w, e_{ow}, e_{og}, e_g)	1.0, 1.7, 2.1, and 3.5
Residual saturations (S_{wr}, S_{owr}, S_{ogr}, S_{gr})	0.2, 0.1, 0.2, and 0.0

Table 8
Pseudo-component data for Case 2.

Component	P_c (psi)	T_c (^{o}R)	V_c (ft3/lb-mol)	M_w (lb/lb-mol)	Ω
C1	667.4	343.4	1.6	16.0	0.008
C3	615.9	666.0	3.3	44.1	0.152
C10	367.7	1120.1	8.4	134	0.443

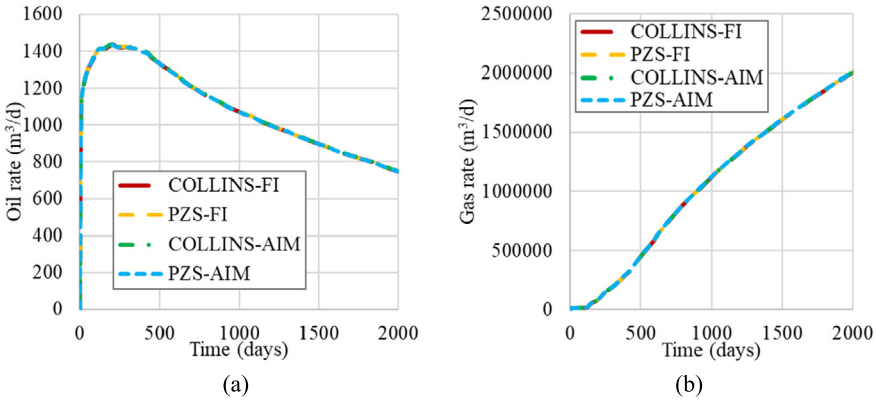

Fig. 22. Comparison of the production rates for Case 2. (a) Oil and (b) gas.

Table 9
CPU Time and numerical performance for Case 2.

Formulation	Normalized CPU time	Solver CPU time (%)	Total number of time-steps	Total number of Newton iterations	Total number of solver iterations
Collins-FI	1.55	68.73	581	4,831	150,230
PZS-FI	1.25	59.60	610	4,732	150,898
Collins-AIM	1.17	54.20	602	5,017	167,340
PZS-AIM	**1.0** (12 h)	45.08	609	4,942	161,584

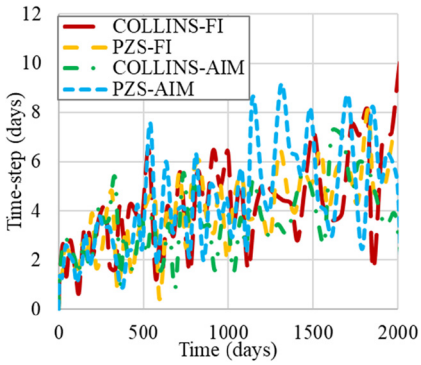

Fig. 23. Comparison of the time-step profile for Case 2.

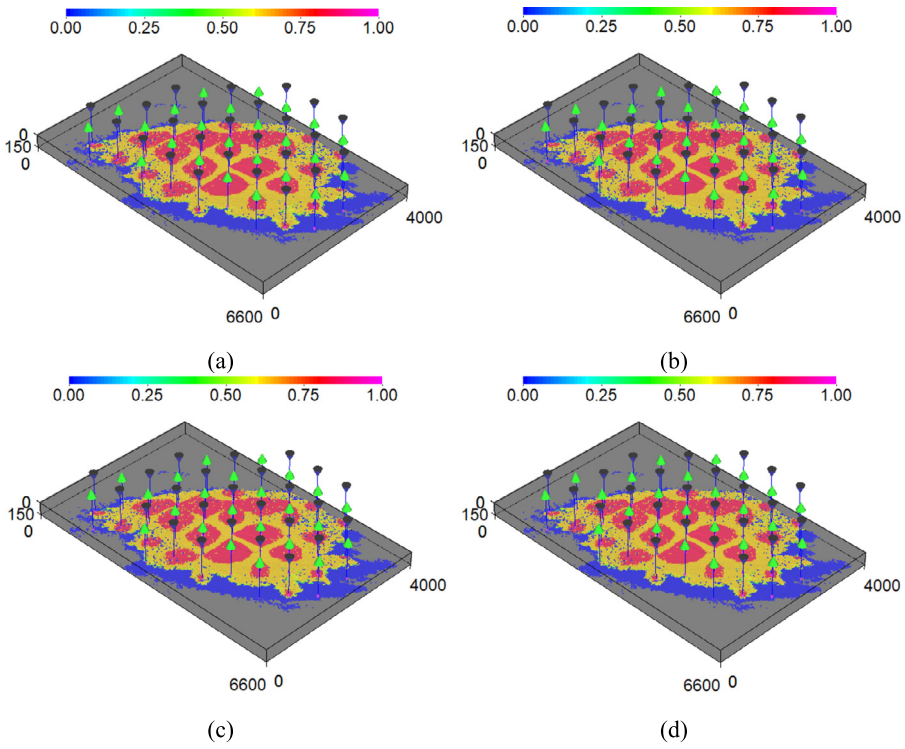

Fig. 24. Comparison of the gas saturation field at 2,000 days for Case 2. (a) COLLINS-FI; (b) PZS-FI; (c) COLLINS-AIM; and (d) PZS-AIM.

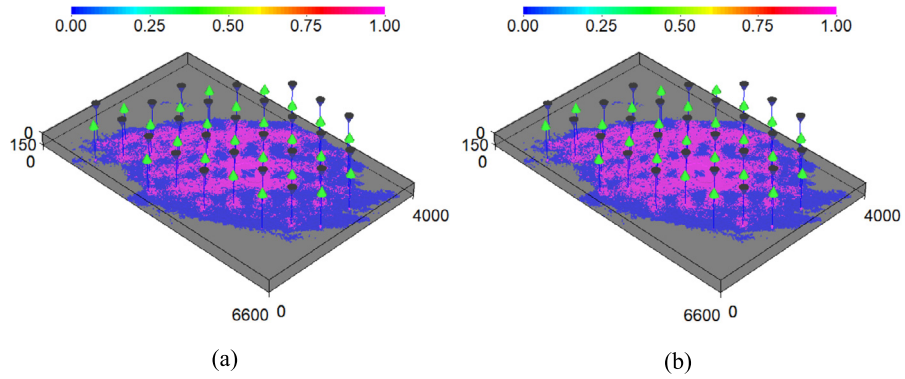

Fig. 25. Implicitness degree at 2,000 days for Case 2. (a) COLLINS-AIM and (b) PZS-AIM.

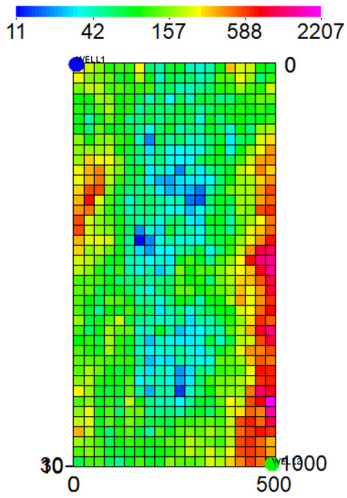

Fig. 26. Absolute permeability field in X and Y directions (mD) for Case 3.

Table 10
Reservoir data for Case 3.

Property	Value
Length, width, and thickness	152.4 m, 304. 8 m, and 6.096 m
Porosity	0.25
Initial water saturation	0.35
Initial pressure	7.58 MPa
Formation temperature	313.71 K
Injector's bottom hole pressure	8.62 MPa
Producer's bottom hole pressure	7.58 MPa
Reservoir's initial composition (CO_2, C_1, C_{2-3}, C_{4-6}, C_{7-15}, C_{16-27}, and C_{28+})	0.0337, 0.0861, 0.1503, 0.1671, 0.3304, 0.1611, and 0.0713
Injection fluid composition (CO_2 and C_1)	0.95 and 0.05

Table 11
Relative permeability data for Case 3.

Property	Value
Model	Corey
End point relative permeabilities (k_{rw}, k_{ro}, k_{rg}, k_{rl})	0.21, 0.7, 0.35 and 0.35
Exponents (e_w, e_{ow}, e_{og}, e_g, e_{lw}, e_{lg})	1.5, 2.5, 2.5, 2.5, 2.5 and 2.5
Residual saturations (S_{wr}, S_{owr}, S_{ogr}, S_{gr}, S_{lwr}, S_{lgr})	0.25, 0.2, 0.2, 0.05, 0.2 and 0.2

Table 12
Pseudo-component data for the BSB oil [42].

Component	P_c (MPa)	T_c (K)	Vc (m^3/mol)	M_w (g/mol)	Ω
CO_2	7.38	304.2	9.43×10^{-5}	44.0	0.225
C_1	4.60	190.6	9.93×10^{-5}	16.0	0.008
C_{2-3}	4.50	344.2	1.81×10^{-4}	37.2	0.1305
C_{4-6}	3.40	463.2	3.06×10^{-4}	69.5	0.2404
C_{7-15}	2.17	605.7	5.99×10^{-4}	141.0	0.6177
C_{16-27}	1.65	751.0	1.13×10^{-3}	281.0	0.9566
C_{28+}	1.64	942.5	2.09×10^{-3}	519.6	1.2683

The reservoir data is presented in Table 10. The relative permeability data for the Corey model [43] are presented in Table 11. Additionally, no dispersion was considered for this case study. The simulation is run for up to 6,000 days (about 3.085 PVI). The properties for each component for the BSB west Texas oil [42] are presented in Table 12.

A comparison of the oil and gas production rates is presented in Fig. 27. From this figure, we can see that there is a good agreement of the production curves obtained with the FI and AIM approaches. There is some deviation from the IMPEC results since its solution uses a much smaller time-step size, which yields a more accurate result in time.

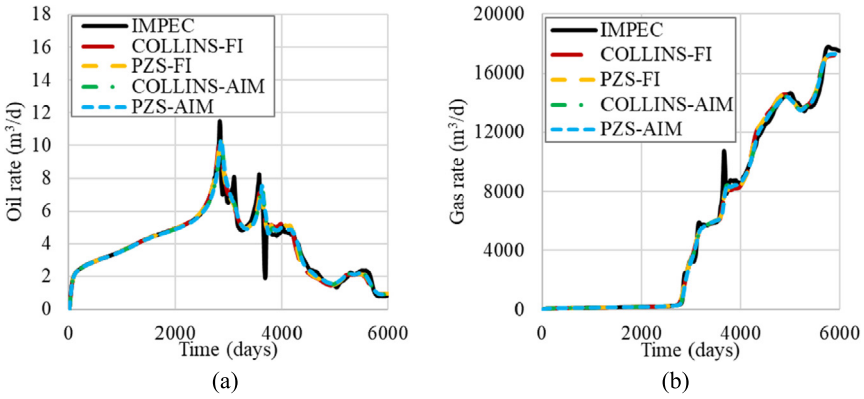

Fig. 27. Comparison of the production rates for Case 3. (a) Oil and (b) gas.

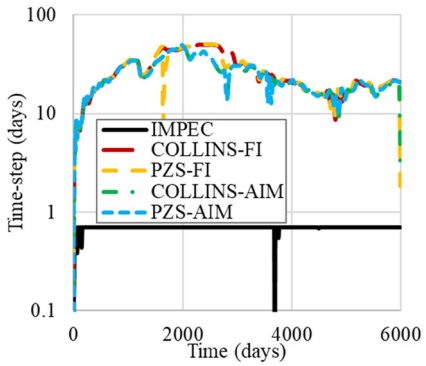

Fig. 28. Comparison of the time-step profile for Case 3.

Table 13
Computational and numerical performance results for Case 3.

Formulation	Normalized CPU time	Solver CPU time (%)	Total number of time-steps	Total number of Newton iterations	Total number of solver iterations
IMPEC	5.20	1.35	8,748	–	149,003
Collins-FI	**1.0** (67 s)	30.98	289	1,042	19,889
PZS-FI	1.01	25.87	296	1,110	20,905
Collins-AIM	1.24	35.36	302	1,118	21,521
PZS-AIM	1.21	29.74	305	1,202	23,172

The time-step profile is presented in Fig. 28. From this figure, we can clearly observe that the FI and AIM approaches used similar time-step profiles. Again, the time-step size for the IMPEC was much smaller than the other aforementioned approaches.

Fig. 29 presents the gas saturation field at 3,000 days of simulation for all formulations tested. It can be observed that a very good agreement of the saturation field is obtained for all the approaches tested. Similar behavior is obtained for the second liquid saturation (Fig. 30) and the water saturation (Fig. 31). Fig. 32 presents the implicitness map for the AIM approaches. Once again, IMPEC cells are marked as zero, while FI gridblocks are marked as one. It can be observed that the implicitness degree covers the whole front.

The cumulative number of Newton iterations, solver iterations, time-steps, and the CPU time are presented in Table 13. Among the formulations tested, the IMPEC approach was slower than any of the AIM and FI approaches. It is interesting to notice, for this case study, that all the AIM approaches are slower than the FI approaches. This happens because the AIM approaches had a high implicitness degree. Such behavior is not desirable for the AIM approach not only because the AIM framework has a computational time overhead due to the switching of gridblocks between explicit and implicit, but the ILU preconditioner structure needs to be recalculated every time a change in the implicitness pattern happens.

Case 4 considers a 3D irregular reservoir with heterogeneous permeabilities and porosity. Thirteen wells are completed with six injectors operating at constant bottom hole pressure and seven producers operating at constant bottom hole pressure. The reservoir is discretized with a $200 \times 200 \times 10$ Cartesian grid with the irregular shape described with inactive cells

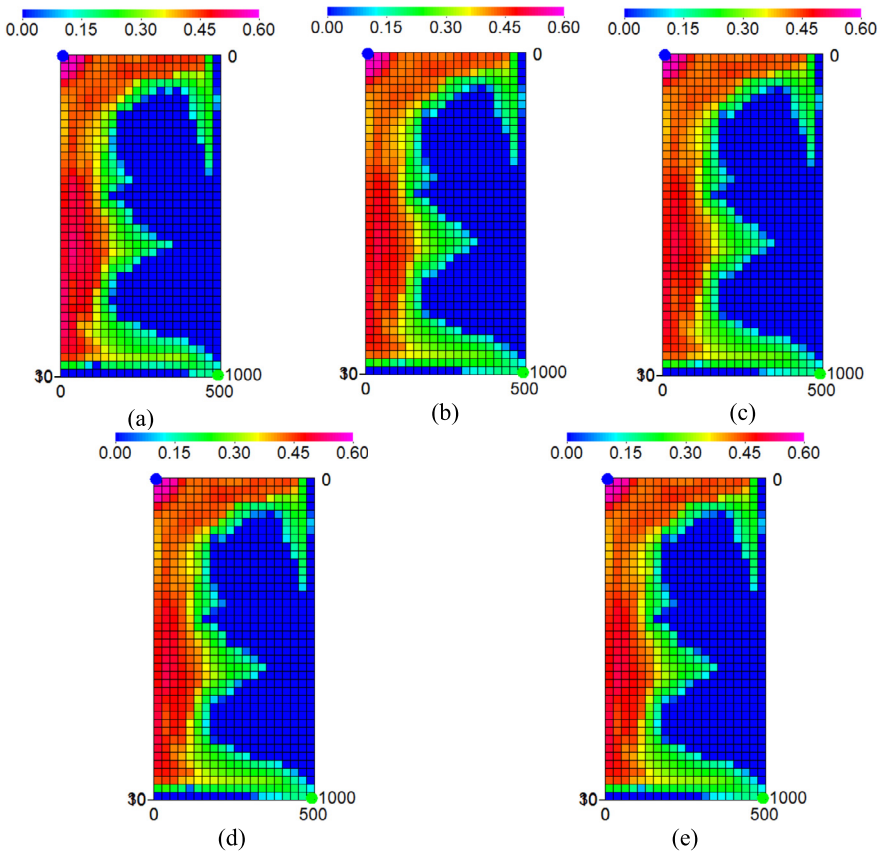

Fig. 29. Comparison of the gas saturation field at 3,000 days for Case 3. (a) IMPEC; (b) COLLINS-FI; (c) PZS-FI; (d) COLLINS-AIM; and (e) PZS-AIM.

Table 14
Reservoir data for Case 4.

Simulation parameters	Value
Reservoir data	
Grid	$200 \times 200 \times 10$ (99,816 active)
Number of wells	13 (6 injector / 7 producer)
Length, width, and thickness	1,219.2 m, 1,219.2 ft, and 60.69 ft
Initial water saturation	0.25
Longitudinal dispersivity	474 m
Transversal dispersivity	4.74 m
Initial pressure	7.58 MPa
Formation temperature	313.7 ^{o}F
Injector's bottom hole pressure	8.62 MPa
Producer's bottom hole pressure	7.58 MPa
Reservoir's initial composition (CO_2, C_1, C_{2-3}, C_{4-6}, C_{7-15}, C_{16-27}, and C_{28+})	0.0337, 0.0861, 0.1503, 0.1671, 0.3304, 0.1611, and 0.0713
Injection fluid composition (C_1, C_3, and C_{10})	0.95 and 0.05
Run data	
Simulation time (days)	2,000
Simulation time (pore volumes)	0.222

(Fig. 33). The BSB west Texas oil [42] is used for this case as well. The permeability field is presented in Fig. 34, while the porosity field is shown in Fig. 35.

The reservoir data considering the physical dispersion is presented in Table 14. The relative permeability curves are based on the Corey model [43] and the parameters used are the same used for Case 3. Similarly, the BSB west Texas oil data given in Table 15 for Case 3 is used. The simulation is performed for up to 2,000 days (about 0.222 PVI).

The IMPEC approach is not presented here since it was unable to complete the simulation. A comparison of the oil and gas production rates is presented in Fig. 36. From this figure, we can see that there is a good agreement of the production curves obtained with the approaches tested.

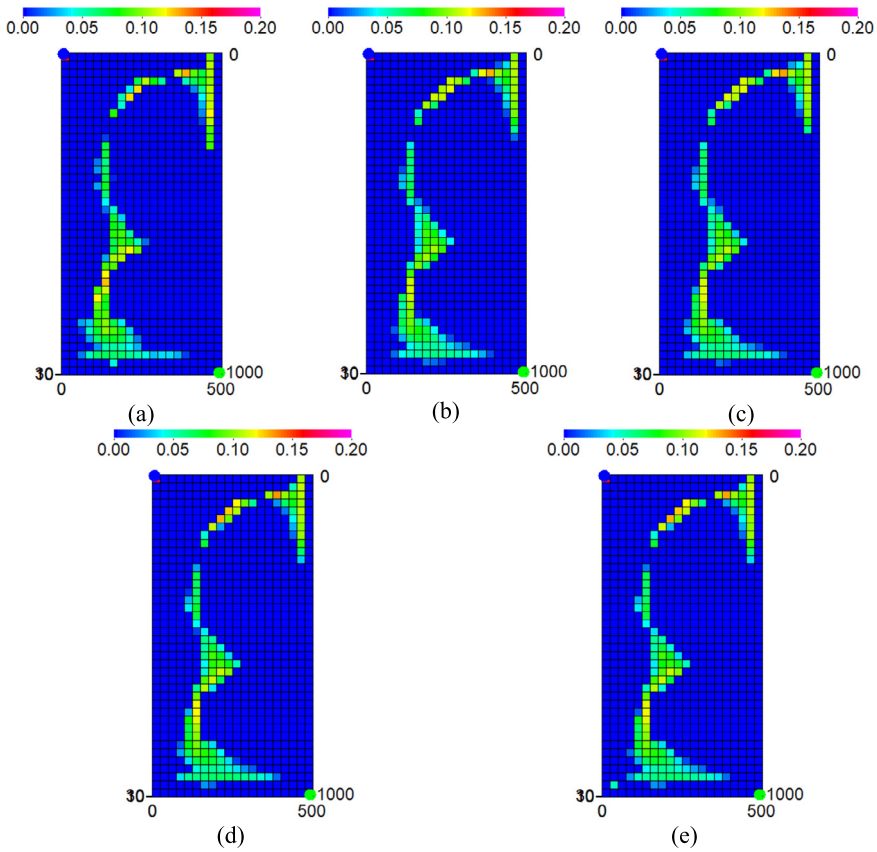

Fig. 30. Comparison of the second liquid saturation field at 3,000 days for Case 3. (a) IMPEC; (b) COLLINS-FI; (c) PZS-FI; (d) COLLINS-AIM; and (e) PZS-AIM.

Table 15
Computational and numerical performance results for Case 4.

Formulation	Normalized CPU time	Solver CPU time (%)	Total number of time-steps	Total number of Newton iterations	Total number of solver iterations
IMPEC	Fail	–	–	–	–
Collins-FI	1.88	28.18	924	1,927	26,638
PZS-FI	1.24	29.49	461	1,550	25,806
Collins-AIM	1.46	2.84	931	1,871	31,191
PZS-AIM	**1.00** (5.0 h)	3.66	511	1,557	31,110

The time-step profile is presented in Fig. 37. From this figure, we can observe that all approaches were able to reach the maximum time-step at certain period, and the run had several time-step cuts.

The gas saturation field and second liquid saturation field at 2,000 days for the different approaches is presented in Figs. 38 and 39, respectively. It can be observed a good agreement of the fields from these figures.

The implicitness degree for each of the approaches with the new switching criteria is presented in Fig. 40.

Table 15 presents the numerical performance of the formulations used in this case. From this table, one can observe that the AIM approaches had a better performance than their corresponding FI approaches. The best approach was the PZS-AIM, followed by the PZS-FI with an overhead of 24%.

7. Conclusions

In this work, a new adaptive implicit formulation and switching criterion for compositional reservoir simulation up to four-phases (three hydrocarbon components plus water) were proposed. The new AIM formulation combined a fully implicit approach based on intensive global variables and the IMPEC approach from Collins et al. [11]. The new switching criterion is an extension of a well stablished stability method originally proposed for up to three-phase systems that has been adjusted to any number of phases. A procedure is presented with the algorithm for performing the proper reduction of variables involved in both IMPEC and FI approaches that compose the new formulation. The new formulation has been applied to

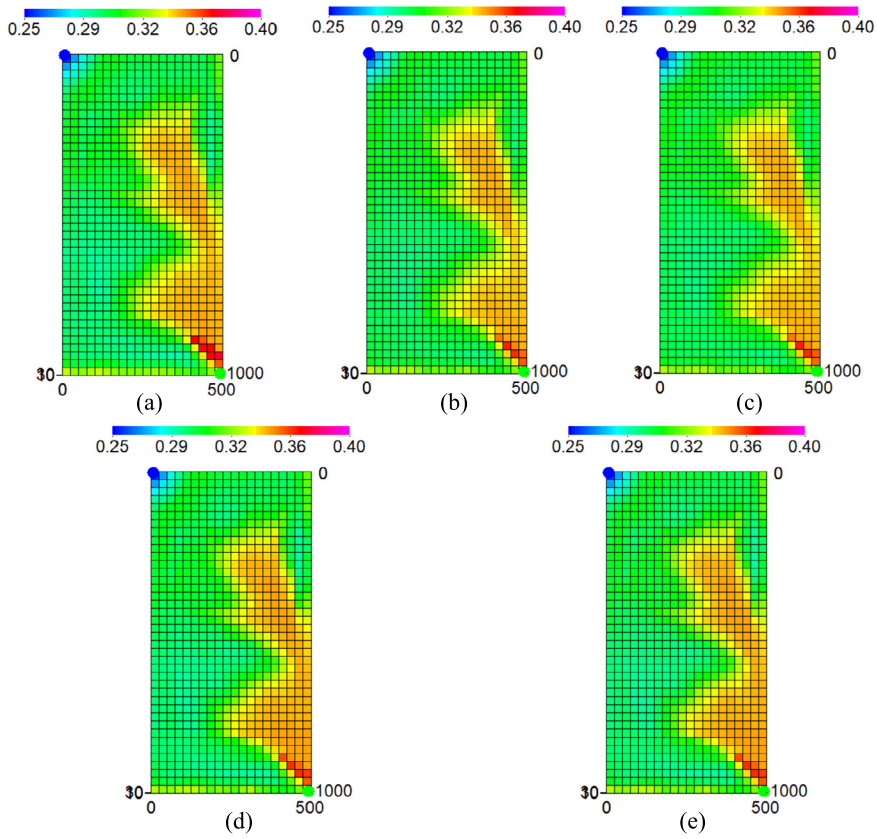

Fig. 31. Comparison of the water saturation field at 3,000 days for Case 3. (a) IMPEC; (b) COLLINS-FI; (c) PZS-FI; (d) COLLINS-AIM; and (e) PZS-AIM.

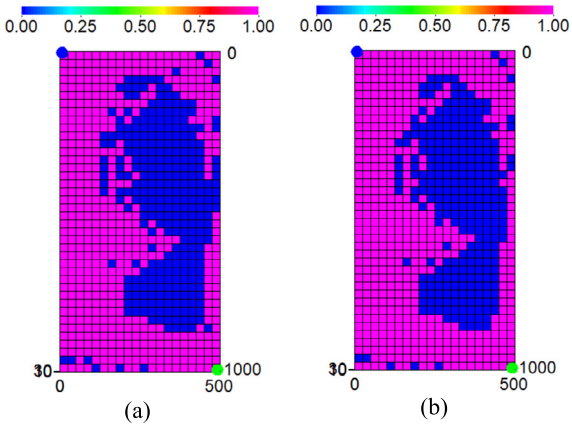

Fig. 32. Comparison of the implicitness map at 3,000 days for Case 3. (a) Collins-AIM and (b) PZS-AIM.

highly complex and heterogeneous reservoirs that strongly impact the numerical performance of the available numerical approaches.

The new formulation was tested and compared with its FI and IMPEC counterparts, and with another AIM. Herein, the case studies presented show that the new AIM is faster than the other AIM proposed by Collins et al. [11]. Also, it was observed that the AIM approaches were superior than the FI approaches when large reservoirs are considered. The new approach was also successful in simulating reservoirs with irregular geometries through the use of the inactive cells approach.

We can conclude that the formulation presented here is a powerful approach to speed up reservoir simulators considering the fluid flow of a large number of phases. Although the overall performance of the AIM approach depends of the reservoir parameters and fluid behavior, the current AIM approach had a superior performance in terms of CPU time for

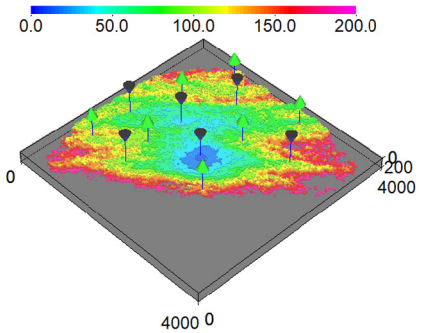

Fig. 33. Depth relative to the reservoir top (ft) for Case 4.

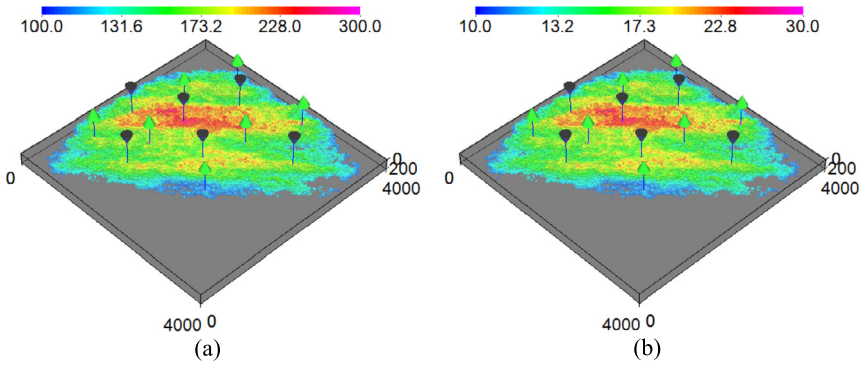

Fig. 34. Absolute permeability fields (mD) for Case 4. (a) *X* and *Y* directions and (b) *Z* direction.

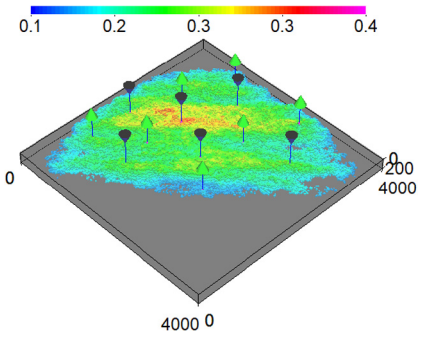

Fig. 35. Porosity field for Case 4.

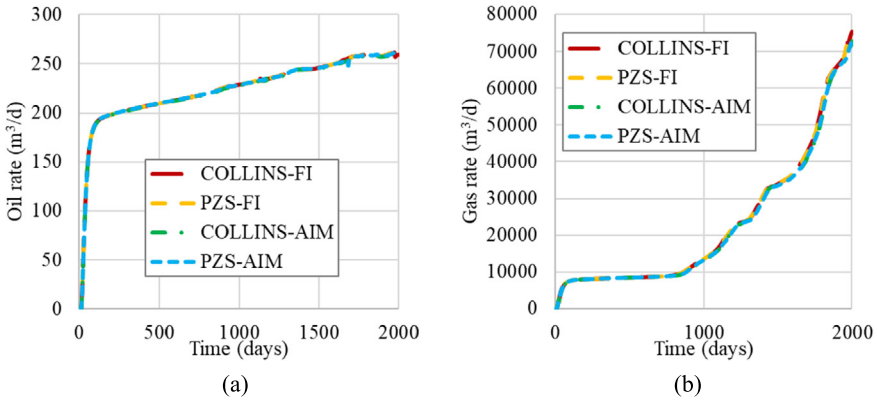

Fig. 36. Comparison of the production rates for Case 4. (a) Oil and (b) gas.

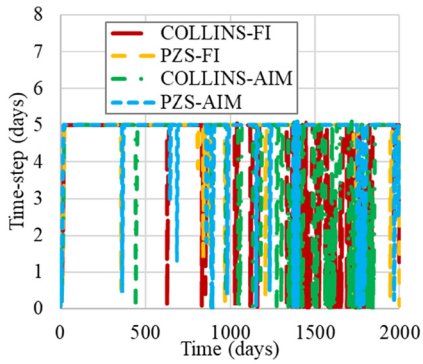

Fig. 37. Comparison of the time-step profile for Case 4.

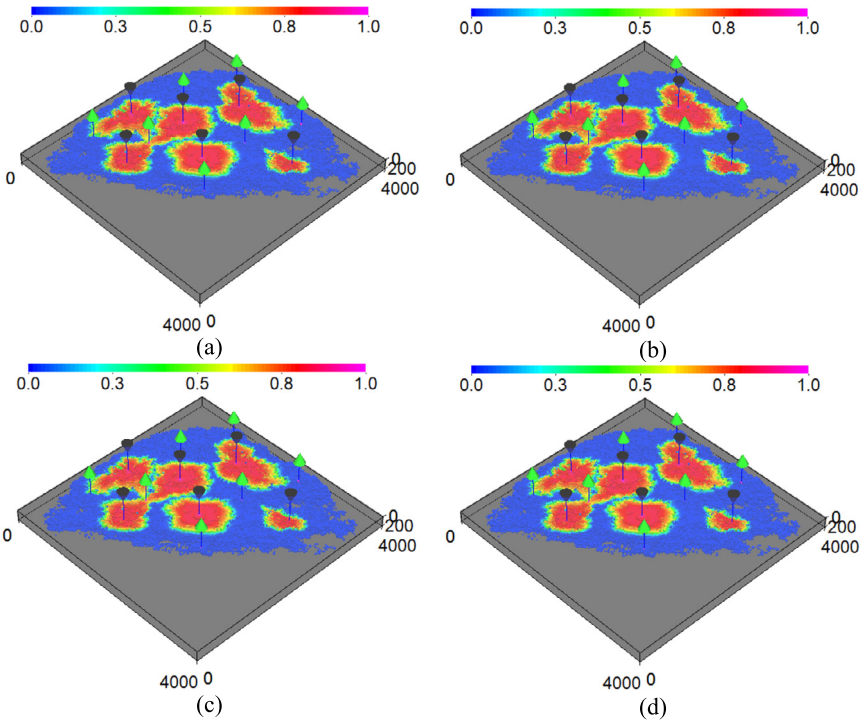

Fig. 38. Comparison of the CO_2 overall concentration field at 2,000 days for Case 4. (a) Collins-FI; (b) PZS-FI; (c) Collins-AIM; and (d) PZS-AIM.

case studies 2 and 4, that had several injecting and producing wells, while case studies 1 and 3 had just one injecting and one producing well. It is important to stress that reservoirs with several wells present several saturation fronts, which demonstrate that the new switching criterion proposed was strong enough to detect the instability regions and switch the gridblocks from IMPEC to FI when the CFL was large and turn them back to IMPEC when the CFL was small.

CRediT authorship contribution statement

Bruno Ramon Batista Fernandes: Methodology, Software, Writing – original draft. **Francisco Marcondes:** Conceptualization, Supervision, Writing – review & editing. **Kamy Sepehrnoori:** Conceptualization, Funding acquisition, Resources, Supervision, Writing – review & editing.

Declaration of competing interest

The authors declare that they have no known competing financial interests or personal relationships that could have appeared to influence the work reported in this paper.

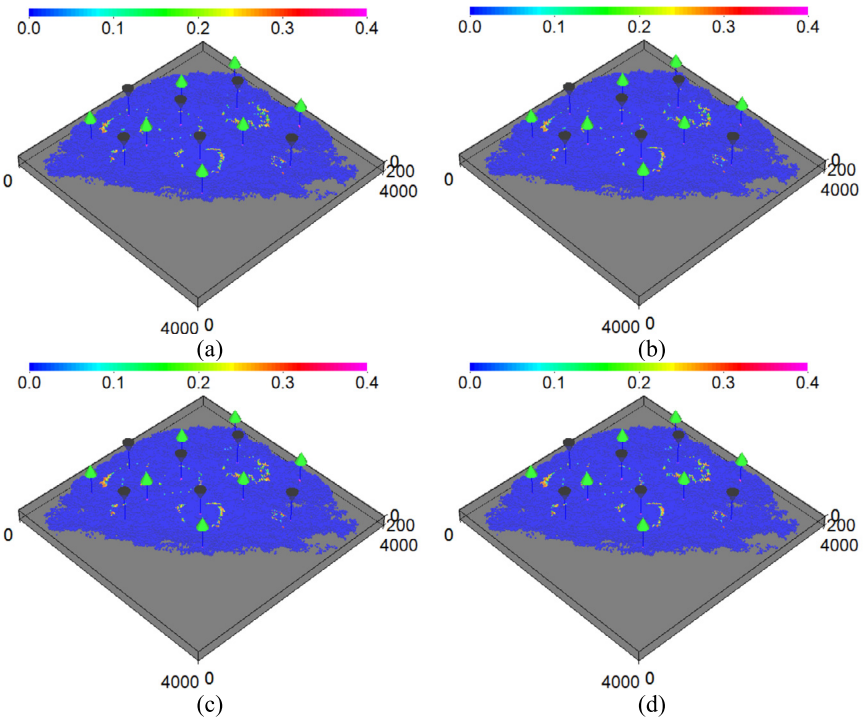

Fig. 39. Comparison of the second liquid overall concentration field at 2,000 days for Case 4. (a) Collins-FI; (b) PZS-FI; (c) Collins-AIM; and (d) PZS-AIM.

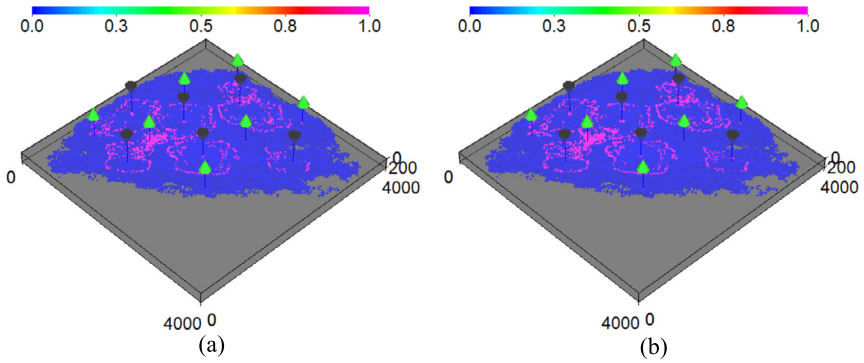

Fig. 40. Comparison of the implicitness field at 2,000 days for Case 4. (a) Collins-AIM and (b) PZS-AIM.

Acknowledgements

The authors would like acknowledge the sponsors of the RS-JIP of the Center for Subsurface Energy and the Environment at The University of Texas at Austin for the financial support. The authors also thank ScienceSoft for providing the S3Graf post-processor. The first and second authors would like to acknowledge CNPq (The National Council for Scientific and Technological Development of Brazil) for its financial support (Grant Nos. 234476/2013-3 and 307427/2018-8, respectively).

References

[1] L.T. Fussell, D.D. Fussell, An iterative technique for compositional reservoir models, Soc. Pet. Eng. J. 19 (1979) 211–220, https://doi.org/10.2118/6891-PA.
[2] G. Acs, S. Doleschall, E. Farkas, General purpose compositional model, Soc. Pet. Eng. J. 25 (1985) 543–553, https://doi.org/10.2118/10515-PA.
[3] L.X. Nghiem, D.K. Fong, K. Aziz, Compositional modeling with an equation of state (includes associated papers 10894 and 10903), Soc. Pet. Eng. J. 21 (1981) 687–698, https://doi.org/10.2118/9306-PA.
[4] L.O.S. Santos, A. Varavei, K. Sepehrnoori, A comparison of various formulations for compositional reservoir simulation, Society of Petroleum Engineers, The Woodlands, Texas, USA, 2013.
[5] L.C. Young, R.E. Stephenson, A generalized compositional approach for reservoir simulation, Soc. Pet. Eng. J. 23 (1983) 727–742, https://doi.org/10.2118/10516-PA.
[6] M.C.H. Chien, S.T. Lee, W.H. Chen, A new fully implicit compositional simulator, in: Society of Petroleum Engineers, Dallas, TX, USA, 1985.
[7] K.H. Coats, An equation of state compositional model, Soc. Pet. Eng. J. 20 (1980) 363–376, https://doi.org/10.2118/8284-PA.

[8] B.R.B. Fernandes, F. Marcondes, K. Sepehrnoori, Development of a fully implicit approach with intensive variables for compositional reservoir simulation, J. Pet. Sci. Eng. 169 (2018) 317–336, https://doi.org/10.1016/j.petrol.2018.05.039.
[9] P. Wang, I. Yotov, M. Wheeler, T. Arbogast, C. Dawson, M. Parashar, K. Sepehrnoori, A new generation EOS compositional reservoir simulator, Part I: formulation and discretization, in: Society of Petroleum Engineers, Dallas, USA, 1997.
[10] H. Cao, Development of techniques for general purpose simulators, PhD Dissertation, Stanford University, 2002.
[11] D.A. Collins, L.X. Nghiem, Y.-K. Li, J.E. Grabonstotter, An efficient approach to adaptive - implicit compositional simulation with an equation of state, SPE Reserv. Eng. 7 (1992) 259–264, https://doi.org/10.2118/15133-PA.
[12] G.W. Thomas, D.H. Thurnau, Reservoir simulation using an adaptive implicit method, Soc. Pet. Eng. J. 23 (1983) 759–768, https://doi.org/10.2118/10120-PA.
[13] G.W. Thomas, D.H. Thurnau, The mathematical basis of the adaptive implicit method, in: Society of Petroleum Engineers, New Orleans, Louisiana, USA, 1982.
[14] P.A. Forsyth, P.H. Sammon, Practical considerations for adaptive implicit methods in reservoir simulation, J. Comput. Phys. 62 (1986) 265–281, https://doi.org/10.1016/0021-9991(86)90127-0.
[15] K.H. Coats, IMPES stability: the CFL limit, SPE J. 8 (2003) 291–297, https://doi.org/10.2118/85956-PA.
[16] K.H. Coats, IMPES stability: selection of stable timesteps, SPE J. 8 (2003) 181–187, https://doi.org/10.2118/84924-PA.
[17] P.A. Forsyth, Adaptive implicit criteria for two-phase flow with gravity and capillary pressure, SIAM J. Sci. Stat. Comput. 10 (1989) 227–252, https://doi.org/10.1137/0910017.
[18] L.S.-K. Fung, D.A. Collins, L.X. Nghiem, An adaptive-implicit switching criterion based on numerical stability analysis, SPE Reserv. Eng. 4 (1989) 45–51, https://doi.org/10.2118/16003-PA.
[19] J. Grabenstetter, Y.-K. Li, D.A. Collins, L.X. Nghiem, Stability-based switching criterion for adaptive-implicit compositional reservoir simulation, in: Society of Petroleum Engineers, Anaheim, USA, 1991.
[20] F. Marcondes, C.R. Maliska, M.C. Zambaldi, A comparative study of implicit and explicit methods using unstructured Voronoi meshes in Petroleum reservoir simulation, J. Braz. Soc. Mech. Sci. Eng. 31 (2009), https://doi.org/10.1590/S1678-58782009000400010.
[21] T.F. Russell, Stability analysis and switching criteria for adaptive implicit methods based on the CFL condition, in: Society of Petroleum Engineers, Houston, USA, 1989.
[22] J.W. Watts, M. Rame, An algebraic approach to the adaptive implicit method, in: Society of Petroleum Engineers, Houston, USA, 1999.
[23] L.C. Young, T.F. Russell, Implementation of an Adaptive Implicit Method, in, in: Society of Petroleum Engineers, New Orleans, Louisiana, USA, 1993.
[24] R. de Loubens, L. Patacchini, A. Moncorge, Adaptive-implicit strategy for treating velocity-dependent mobilities in reservoir simulation, in: SPE Reserv. Simul. Symp., Society of Petroleum Engineers, The Woodlands, Texas, USA, 2013.
[25] L.D. Carciopolo, M. Cusini, L. Formaggia, H. Hajibeygi, Adaptive multilevel space-time-stepping scheme for transport in heterogeneous porous media (ADM-LTS), J. Comput. Phys. X 6 (2020) 100052, https://doi.org/10.1016/j.jcpx.2020.100052.
[26] R.L. Burden, J.D. Faires, A.M. Burden, Numerical Analysis, Tenth edition, Cengage Learning, Boston, MA, 2016.
[27] Y. Chang, Development and application of an equation of state compositional simulator, PhD Dissertation, The University of Texas at Austin, 1990.
[28] J. Bear, Dynamics of Fluids in Porous Media, Dover, New York, 1988.
[29] L.W. Lake, Enhanced oil recovery, in: Society of Petroleum Engineers, Richardson, Tex, 2010.
[30] L.C. Young, Use of dispersion relationships to model adverse-mobility-ratio miscible displacements, SPE Reserv. Eng. 5 (1990) 309–316, https://doi.org/10.2118/14899-PA.
[31] D.-Y. Peng, D.B. Robinson, A new two-constant equation of state, Ind. Eng. Chem. Fundam. 15 (1976) 59–64, https://doi.org/10.1021/i160057a011.
[32] M.L. Michelsen, The isothermal flash problem. Part I. Stability, Fluid Phase Equilib. 9 (1982) 1–19, https://doi.org/10.1016/0378-3812(82)85001-2.
[33] D.R. Perschke, Equation of state phase behavior modelling for compositional simulator, PhD Dissertation, The University of Texas at Austin, 1988.
[34] J.A. Trangenstein, Customized minimization techniques for phase equilibrium computations in reservoir simulation, Chem. Eng. Sci. 42 (1987) 2847–2863, https://doi.org/10.1016/0009-2509(87)87051-3.
[35] R.K. Mehra, R.A. Heidemann, K. Aziz, An accelerated successive substitution algorithm, Can. J. Chem. Eng. 61 (1983) 590–596, https://doi.org/10.1002/cjce.5450610414.
[36] B.R.B. Fernandes, Development of adaptive implicit chemical and compositional reservoir simulators, PhD Dissertation, The University of Texas at Austin, 2019.
[37] Y. Saad, M.H. Schultz, GMRES: a generalized minimal residual algorithm for solving nonsymmetric linear systems, SIAM J. Sci. Stat. Comput. 7 (1986) 856–869, https://doi.org/10.1137/0907058.
[38] S. Balay, M.F. Adams, J. Brown, P. Brune, K. Buschelman, V. Eijkhout, W.D. Gropp, D. Kaushik, M.G. Knepley, L.C. Mcinnes, K. Rupp, B.F. Smith, H. Zhang, PETSc User's Manual, Argonne National Laboratory, USA, 2013.
[39] H.L. Stone, Estimation of three-phase relative permeability and residual oil data, J. Can. Pet. Technol. 12 (1973), https://doi.org/10.2118/73-04-06.
[40] J.E. Killough, C.A. Kossack, Fifth comparative solution project: evaluation of miscible flood simulators, in: Society of Petroleum Engineers, San Antonio, Texas, 1987.
[41] R. Okuno, Modeling of multiphase behavior for gas flooding simulation, PhD Dissertation, The University of Texas at Austin, 2009.
[42] S.A. Khan, G.A. Pope, K. Sepehrnoori, Fluid characterization of three-phase CO_2/Oil mixtures, in: Society of Petroleum Engineers, Tulsa, Oklahoma, USA, 1992.
[43] A.T. Corey, Mechanics of Immiscible Fluids in Porous Media, 2nd ed, Water Resources Publications, Littleton, Colorado, USA, 1986.